The Development of Microtubular Arrays in the Germ Tissue of an Insect Telotrophic Ovary

by

Gunnar Valdimarsson

A thesis
presented to the University of Manitoba
in partial fulfillment of the
requirements for the degree of
Master of Science
in
Zoology

Winnipeg, Manitoba

ISBN 0-315-37462-4

THE DEVELOPMENT OF MICROTUBULAR ARRAYS IN THE GERM TISSUE OF AN INSECT TELOTROPHIC OVARY

by

GUNNAR VALDIMARSSON

A thesis submitted to the Faculty of Graduate Studies of the University of Manitoba in partial fulfillment of the requirements of the degree of

MASTER OF SCIENCE

ABSTRACT

The germ tissue of the adult ovariole of Rhodnius prolixus contains extensive microtubular arrays, localized in the trophic core and cords. The development of these arrays during the larval-adult transformation was investigated using light and transmission electron microscopy. Tubulin levels were assessed using polyacrylamide gel electrophoresis and electrophoretic transfer to nitrocellulose.

PEG and DGD embedding media were compared for the indirect immunofluorescence of tubulin. DGD was deemed a more suitable medium based on sectioning ease and section quality.

Microtubular arrays were first detected in the trophic cords and presumptive core 6 days before the molt. Cord microtubules increase in length and numbers as the trophic cords grow. Three microtubule packed growing cords have formed by 1 day post molt. The microtubule distribution in the presumptive core is non-uniform. Microtubule packed areas are interspersed with areas devoid of microtubules. The adult core begins forming between 1 day before molt and molting. This early adult core arises from the fusion of the anterior portions of microtubule packed trophic cords. A fully mature adult trophic core is not present by 2 days

post molt. The microtubule packing density in the core increases from 2 days before to 2 days post molt. Tubulin increases from 6 days before molt to 3 days before molt and possibly to 1 day before molt.

ACKNOWLEDGEMENTS

First I would like to thank Dr. E. Huebner for his patient guidance and support during the course of my stay in his lab. I would also like to thank Greg Kelly, Bill Diehl-Jones, and Sandra Graham for numerous discussions, scientific or otherwise. I also like to thank Þórarinn Sveinsson, Odd Bres, Dean Berezanski, and Bernie McIntyre for technical advice. I would like to thank the examining committee, Dr. J. G. Eales, and Dr. C. Braekevelt for their contributions. I would also like to acknowledge financial assistance from the following sources: NSERC research grant to Dr. E. Huebner, teaching assistantships from the Department of Zoology, Grant-in-Aid of Research from Sigma Xi, and the Gunnar Simundson Memorial Scholarship from Icelandic-Canadian Frón. I wish to thank my parents and my mother-in-law for all their help and encouragement. Finally I would like to extend a very special thank you to my wife, Lorna Jakobson, for her constant support and for making it all worth while.

TABLE OF CONTENTS

INTRODUCTION

Microtubules (MTs) are ubiquitous cell constituents, found in all eukaryotic cells with the exception of the anucleate mammalian erythrocyte (Dustin, 1984). MTs along with the two other ubiquitous eukaryotic filament classes, microfilaments and intermediate filaments, play an important role in a number of cellular processes such as: the maintenance of cell shape (Tucker, 1979; Kirschner and Mitchison, 1986; Murphy et al., 1986), cell locomotion (Drubin et al., 1985; Singer and Kupfer, 1986), intracellular transport (Hyams and Stebbings, 1979a; Schliwa, 1982,1984; Miller and Lasek, 1985), and cell division (Inoué and Dan, 1951; Pickett-Heaps, 1984; Mitchison et al., 1986; Gorbsky et al., 1987).

Since MTs were first brought into prominence in 1963 (Ledbetter and Porter), voluminous literature has amassed about these cell constituents. Structurally MTs are made up of 4-5nm subunits (for review see Amos et al., 1976). Biochemically these subunits are of equal molecular weight (MW), α and β, which make up the heterodimer tubulin, the constituent protein of MTs (for review see McKeithan and Rosenbaum, 1984).

The insect telotrophic meroistic ovary possesses one of the most extensive MT systems yet described. This fact

combined with the thorough morphological and physiological information available on this tissue make it an ideal model to study MTs in an integrated multicellular system. To provide background information relevant to the thesis problem a brief review on the meroistic telotrophic ovary and what is known about its MT component is useful.

In the meroistic ovary, the germ cells become differentiated into two functionally distinct cell types, nurse cells and oocytes (King and Büning, 1985). In telotrophic meroistic ovaries all the nurse cells are housed anteriorly but are connected to individual oocytes via accentuated cytoplasmic bridges, the trophic cords (Telfer, 1975; Huebner, 1984a; King and Büning, 1985). There are three subtypes of telotrophic ovaries, one in polyphagous Coleoptera, one in Megaloptera/Raphidoptera, and one in Hemiptera (Bonhag, 1958; Büning, 1972, 1979a,b, 1980; Huebner and Anderson, 1972a,b,c). Only the hemipteran type has the extensive MT system.

The morphology of the Rhodnius adult telotrophic ovary is well established (Huebner, 1984a). Only the relevant features of the nurse cells and the trophic cords will be mentioned here. Each of the two ovaries consists of seven ovarioles. All the nurse cells are housed in an anterior syncytial chamber, the tropharium. The nurse cells are organized around a central nucleus- and membrane-free cylindrical area, the trophic core. These nurse cells are syncytial and are all connected to the core by lateral

channels. The trophic cords branch off the base of the trophic core and extend posteriorly to the oocytes. A remarkable feature of this interacting cell system is the massive array of parallel MTs, arranged longitudinally in the trophic core and cords. Some MTs also occur in the lateral channels. The only organelles in the core and cords, besides MTs, are ribosomes and mitochondria (Huebner and Anderson, 1970, 1972c; Huebner, 1981, 1984a). A similar situation exists in other hemipterans. However, MT density, size of transported particles, and time of trophic cord closure vary with species (Brunt, 1970; MacGregor and Stebbings, 1970; Hyams and Stebbings, 1977a; Bennett and Stebbings, 1979; Huebner, 1981,1984a).

In meroistic ovaries, the oocyte genome remains relatively inert during oogenesis, whereas the nurse cell genome is responsible for supplying most of the informational macromolecules needed by the oocyte (Davidson, 1986). The presence of a macromolecular transport from nurse cell to oocytes and the identity of the molecules transported has been determined in a number of hemipteran genera. The transport of RNAs and proteins has been demonstrated in Dysdercus (Brunt, 1970; Duspiva et al., 1973; Winter, 1974; Winter et al., 1977), Pyrrochoris (Mays, 1972), Gerris (Eschenberg and Dunlap, 1966; Choi and Nagl, 1977), Notonecta (MacGregor and Stebbings, 1970; Stebbings, 1971; Bennett and Stebbings, 1979; Sharma and Stebbings, 1985), Oncopeltus (Bonhag, 1955; Zinsmaster and Davenport,

1971; Davenport, 1974,1976; Schreiner, 1977; Capco and Jeffrey, 1979), and Rhodnius (Anderson and Beams, 1956; Vanderberg, 1963; Huebner and Anderson, 1970, 1972b,c; Huebner, 1984a).

Since MTs were first described in the trophic core and cords of hemipteran ovarioles (Hamon and Folliot, 1969; Brunt, 1970; Huebner and Anderson, 1970; MacGregor and Stebbings, 1970), considerable effort has been directed at understanding the various structural, biochemical, and physiological properties of the MTs per se and in this system in particular. The MT substructure has been investigated by freeze-etching (Stebbings and Willison, 1973) and freeze-substitution (Indi et al., 1985) techniques. These studies show that the ovarian MTs are structurally identical to MTs in other systems. A clear zone into which no cytoplasmic structures encroach surrounds each MT (MacGregor and Stebbings, 1970; Stebbings and Willison, 1973; Huebner, 1981). This clear zone is obliterated by treatments which depolymerize the MTs, thus indicating that it is MT dependent (Stebbings and Bennett, 1976). It has been hypothesized recently that the clear zone is the result of an electrostatic repulsion between the MTs and the surrounding cytoplasmic structures (Stebbings and Hunt, 1982). The MTs are depolymerized by vinblastine (VBL) treatment both in Notonecta (Stebbings, 1971, 1975), and in Rhodnius (Huebner and Anderson, 1970; Huebner, 1981). Cold and colchicine treatments do not destroy the MTs in

intact Rhodnius ovarioles (Huebner, 1981, 1984a) or in isolated trophic cords from Notonecta (Hyams and Stebbings, 1979b), but do destroy the MTs in intact Notonecta ovarioles (MacGregor and Stebbings, 1970; Stebbings and Bennett, 1976).

Biochemical studies show that the main component of the trophic cords is tubulin (Hyams and Stebbings, 1979b; Sharma and Stebbings, 1985). Microtubule-associated proteins (MAPs) may also be present (Stebbings et al., 1986). Exogenous dynein has been found to bind to Notonecta MTs (Stebbings and Hunt, 1985) but no endogenous dynein was identified (Hyams and Stebbings, 1979b).

Cord MT packing density is species specific and is correlated with the size of transported particles (Hyams and Stebbings, 1977a). In Dysdercus the MT packing remains constant as the cords enlarge indicating that MTs are assembled at the same rate as the cords grow (Hyams and Stebbings, 1979b). Cord MT packing, however, increases dramatically upon loss of contact with the oocyte (Hyams and Stebbings, 1979b; Bennett and Stebbings, 1979).

MTs possess intrinsic polarity, which arises from the mechanism by which they assemble from tubulin subunits (Dentler et al., 1974; Bergen and Borisy, 1980). In vivo the assembly end or + end of an MT is free whereas the disassembly end or - end is usually embedded in a microtubule organizing center (MTOC) (Tucker, 1979,1984; Kirschner and Mitchison, 1986). Two methods have been

devised to determine MT polarity, the dynein decoration technique (Haimo et al., 1979; Haimo, 1982), and the hook decoration technique (Euteneur and McIntosh, 1980,1981a,b; McIntosh and Euteneur, 1984). The hook decoration technique has shown that the + end of the cord MTs in Notonecta is located at the anterior end of the cord (Stebbings and Hunt, 1983).

With this background information on the telotrophic ovariole and MTs, I can now focus on the research problems of this thesis. The initial objective of this study was to determine the precise developmental timing and pattern of MT appearance in the Rhodnius prolixus trophic core and cords. However, before this objective could be addressed the problem of visualizing MTs in a multicellular system had to be solved. The purpose of the research reported here was therefore twofold: (A) evaluation and modification of methods for visualizing MTs in the insect ovariole; (B) determination of the appearance, orientation, and relative numbers of MTs in the trophic core and cords during the larval-adult transformation.

The choice of visualization methods is of prime importance when studying MTs in a multicellular system. MTs are visible in the transmission electron microscope (TEM) but only at high magnification, making it difficult to discern their overall distribution. Indirect immunofluorescence techniques can specifically render MTs visible in the light microscope. These methods were,

however, primarily developed for use on tissue culture cells in vitro. Only recently have there been attempts to apply these methods to embedded and sectioned material. These methods make it possible to localize cytoskeletal elements in cells, in situ, with minimal loss of structural integrity. Methods that have been attempted include: (1) vibratome sectioning of unembedded tissue (Matus et al., 1981); (2) paraffin embedding and sectioning (Bussolati et al., 1980; Kramer, 1981; Valnes and Brandtzaeg, 1981); (3) thick cryosectioning of frozen tissues (Franke et al., 1978); (4) thin cryosectioning of frozen tissues (Coudrier et al., 1982; Geuze et al., 1981); (5) plastic embedding and semi-thin sectioning (Rodning et al., 1980; Hogan and Smith, 1982); and (6) polyethylene glycol (PEG) embedding and semi-thin sectioning (Repetto-Antoine et al., 1982; Wolosewick and De Mey, 1982; Parysek et al., 1984). Because of section thickness, techniques (1), (2), and (3) do not give sufficient resolution. Both (3) and (4) are undesirable for MT research since they involve cold treatment and most cytoplasmic MTs are cold labile (Webb and Wilson, 1981). Both (5) and (6) offer good structural preservation and optical resolution. Plastics, however, impart high autofluorescence to the tissue, and it is also necessary to remove the plastic from the sections to maximize antibody-antigen contact (Watson, 1984). Plastic removal methods require that the sections be incubated in saturated NaOH in absolute ethanol, a very harsh treatment which leads to

uncertaintity about preservation of antigenic determinants. PEG therefore appeared to be the best suited embedding medium for the purpose of this study.

Recently the use of diethylene glycol distearate (DGD), an easily removable embedding medium, has been reported for TEM (Capco et al., 1984; Capco and McGoughey, 1986). This material appeared to offer all the features which made PEG suitable while lacking some of its undesirable properties. DGD has not been used, to my knowledge, in immunofluorescence localization of cytoskeletal proteins before. One report has appeared on the use of DGD in direct immunofluorescence microscopy (Lacy and Davies, 1959), and another on its use in indirect immunofluorescence microscopy (Taleporos, 1974).

In summary, the methodological objectives of the present study were: (1) to adapt the published DGD methodology for use in indirect immunofluoresence microscopy, and to evaluate its potential usefulness in such applications; and (2) to compare the qualities of PEG and DGD as embedding media for indirect immunofluorescence.

The general morphogenetic events associated with the larval-adult ovarian transformation in Rhodnius has been studied at the ultrastructural level (Huebner and Anderson, 1972c; Lutz and Huebner, 1980, 1981). This background information, which is not available for other hemipterans, and the extensive background already available on the adult ovary, makes the Rhodnius ovariole ideal for studying the

developmental appearance of MTs in the trophic core and cords.

The syncytium of nurse cells and oocytes arises as a consequence of incomplete cytokinesis during mitotic growth in the five larval stadia (Buxton, 1930; Huebner, 1982). The major larval-adult ovarian transformation takes place during the fifth instar. At the beginning of the fifth stadium all the germ cells are arranged around the larval trophic core, and the core itself consists of a tortuous arangement of cell processes (Lutz and Huebner, 1980, 1981). Late in the stadium massive restructuring occurs which results in large core areas free of membranes. The oocytes become detectably differentiated and localized at the base of the tropharium about midway through the stadium. They do, however, retain their connection to the trophic core via elongating cell bridges which thus become parts of the trophic cords. Several of these oocytes initiate pre-vitellogenic growth at this stage. Weak birefringence was observed in the trophic core and cords a few days before the adult molt and this increased in intensity until a few days post adult molt. This was presumed to be due to the establishment of MTs within these structures. It was concluded that MT development represented the final step in the production of a functional adult ovariole (Lutz and Huebner, 1981). A fundamental question which has not been addressed, is whether or not there is a relationship between the onset of nurse cell-oocyte transport and the

establishment of the MT array in the trophic core and cords. Data on the larval-adult transformation with respect to MT assembly and organization are scant. Determination of the temporal sequence of MT development in the trophic cords and core during the larval-adult transformation is necessary.

Thus the biological objectives of the present study were: (1) to determine the developmental timing and pattern of appearance of MT arrays in the trophic core and cords of Rhodnius prolixus ; and (2) to qualitatively compare the levels of tubulin present in the ovaries through the period of MT appearance.

MATERIALS AND METHODS

Animal-rearing methods

The Rhodnius prolixus colony was kept at 26°C and high relative humidity by established methods (Huebner and Anderson, 1972c). Non-fed, newly molted, fifth instars were selected for experiments. To obtain animals developing relatively synchronously, only animals within a set weight range were used. Individual animals were weighed prior to being fed and again 48 hours post-feed. The pre-feed weight range used was 0.055±0.006g and the post-feed weight range used was 0.215±0.022g. The animals were kept in jars in groups of 20.

Dissection methods

The ovaries were dissected out with the animal immersed in Rhodnius saline (Maddrell, 1969), and then transferred to a 35mm Petri dish containing calcium-free Rhodnius saline supplemented with 2.0mM of the calcium chelating agent ethyleneglycol-bis-(β-aminoethyl ether)-N, N, N', N'-tetraacetic acid (EGTA). The tracheoles and the major ovarian sheaths were removed with a pair of fine forceps and the ovarioles separated. For TEM and immunofluorescence microscopy the ovarioles were not dissected further but for

live observations and biochemical analysis the ovariole sheaths were also removed, using fine forceps.

Staging of ovarioles

Previous studies on the Rhodnius larval-adult ovarian transformation have used the time of feeding of the fifth instar as a temporal reference point (Lutz and Huebner, 1980, 1981). These studies found that the fifth instars molted into adults 21 days post feed (dpf). During the early phase of the present study it became apparent that this pattern had changed and that the time interval from feeding to molt was quite variable, within as well as between batches of animals fed at the same time. For example, for the three batches of animals for which accurate data were collected, the average molting time was 26 dpf and the range 24 to 28 days. It therefore became necessary to devise a different time frame. I decided to use the time of molting into adult as a reference point to stage the development into days (i. e. 24 hour periods). A particular animal was therefore either designated n days before molt (n dbm) or n days post molt (n dpm). Ovaries to be examined post molt were obtained by simply checking the jars every 24 hours and putting aside animals which had molted during the preceding 24 hour period. Timing of ovaries to be examined before molt was determined by leaving out a few animals to molt from each batch. From these the average molting time was calculated and used as the reference point. The stage

was then arrived at by counting backwards the number of days between the time of sacrifice and the average molting time for that batch.

Observations were made with polarizing microscopy on live ovarioles daily from 8 dbm to 2 dpm. Ovarioles were examined with immunofluorescence microscopy daily from 4 dbm to 2 dpm. Four stages were examined with the TEM; 2 dbm, 0 dpm, 1 dpm, and 2 dpm. The biochemical comparison of tubulin was done for each day from 6 dbm to 1 dbm.

Observations of live ovarioles

Polarizing microscopy was used to observe birefringence in the trophic core and cords. Desheathed ovarioles were transferred to a drop of calcium-free Rhodnius saline containing 2.0mM EGTA on a glass microscope slide. Two to three ovarioles were mounted per slide. To prevent excessive flattening of the tissue, a small amount of vaseline was applied to each corner of the coverslip for support. The preparation was then viewed and photographed on a Zeiss Photomicroscope 11 equipped with a polarizer and an analyzer.

Brightfield microscopy and TEM

The primary fixative used was a MT stabilizing fixative consisting of 3.0% v/v glutaraldehyde in 60.0mM piperazine-N, N'-bis(2- ethanesulfonic acid) (PIPES), 25.0mM N-2- hydroxyethylpiperazine-N'-2-ethanesulfonic acid (HEPES) pH 6.9, 1.0mM $MgSO_4$, 2.0mM EGTA, 1.0mM guanosine 5'-triphosphate (GTP), 0.5% w/v tannic acid (TA), and 0.05% w/v Saponin (Luftig et al., 1977; Schliwa and van Berkom, 1981; Maupin and Pollard, 1983; Watson and Huebner, 1986).

The ovarioles were fixed for 1 hour, washed in the fixative buffer without GTP, TA, and Saponin for 30 minutes and then postfixed in 0.5% w/v osmium tetroxide in sodium cacodylate buffer, pH 7.2, for 30 minutes. The fixation, washing, and postfixation steps were carried out at room temperature. Following postfixation the ovarioles were rapidly dehydrated in a graded series of ethanol concentrations, 70%, 80%, 95%, 100%, at -20°C. The tissue remained in each concentration for about 30 seconds until reaching 100% where it remained for 15 minutes. A total of four 15 minute changes of 100% were used at room temperature. The ovarioles were then immersed in a 1:1 mixture of 100% ethanol and propylene oxide for 15 minutes, followed by two changes of pure propylene oxide, 15 minutes each. This was replaced with a 1:1 infiltration mixture of propylene oxide and Epon-Araldite (Anderson and Ellis, 1965). Infiltration was carried out for 24 hours. Embedding in flat moulds with fresh Epon-Araldite followed

infiltration, and the plastic was cured at60 °C for at least 48 hours.

For brightfield microscopy semi-thin (1.0μm) Epon-Araldite sections were cut on glass knives using a Sorvall Porter Blum MT2-B ultramicrotome. The sections were stained in 1.0% w/v toluidine blue in 1.0% w/v sodium borax, mounted in immersion oil, and viewed and photographed on a Zeiss Photomicroscope 11.

For TEM thin Epon-Araldite sections were cut with glass knives on the Sorvall Porter Blum MT2-B ultramicrotome, picked up on 150 mesh grids, stained for 30 minutes in a saturated solution of uranyl acetate in 50% ethanol,and then for 3 minutes in lead citrate (Reynolds, 1963). The grids were examined and photographed on AEI 6B or AEI 801S transmission electron microscopes at 60KV accelerating voltage.

Estimates of MT density in the trophic core were obtained from electron micrographs of transverse sections through the core. A cross-diagonal pattern of five squares was placed on a micrograph of known magnification and the number of MTs in each square was counted. The MT number in the five squares was averaged and the resulting number was divided by the true area of a square in μm^2 These values were then averaged for each stage examined. One to three ovarioles were counted for each stage. For each ovariole examined two to four different areas within the core were counted.

Immunofluorescence microscopy methods

Four different fixatives were evaluated. All fixatives were made up in a buffer consisting of 60.0mM PIPES, 25.0mM HEPES, 10.0mM EGTA, 2.0mM $MgCl_2$, pH 6.9 (PHEM buffer) (Schliwa and van Berkom, 1981) with 1.0mM GTP added. The fixatives were as follows: (1) 1.0% w/v paraformaldehyde; (2) 1.0% w/v paraformaldehyde + 0.5% v/v glutaraldehyde; (3) 3.0% w/v paraformaldehyde + 0.1% v/v glutaraldehyde; (4) 3.0% w/v paraformaldehyde + 0.5% v/v glutaraldehyde. The tissue was fixed for 1/2-1 hour, washed in PHEM buffer for 1/2-1 hour and then dehydrated in an ascending concentration series of ethanol as described above. Fixation and washing was done at room temperature. This procedure was used for both PEG and DGD embedding. For fixative evaluation some ovarioles were embedded in Epon-Araldite, semi-thin sectioned, and stained as above.

The methods used for PEG embedding and sectioning involve modifications on the original PEG procedures (Wolosewick, 1980; Wolesewick and De Mey, 1982; Parysek et al., 1984). A 4:1 mixture of PEG 3350 (MW 3,000-3,700) and PEG 1450 (MW 1,300-1,600) (J. T. Baker Chemical Co.) was kept molten at 55°C in the oven. The final change of 100% ethanol was replaced with a 1:1 mixture of 100% ethanol and PEG mixture and the vial placed in a 55°C oven for 4 hours. This was followed by pure PEG mixture overnight. Ovarioles were individually embedded in fresh PEG mixture in Micromold® capsules (SPI Supplies Ltd.) and the PEG was then allowed to harden at room temperature.

After removing the blocks from the moulds the blocks were mounted on wooden stubs with a bit of molten PEG. Semi-thin sections (2.0μm) were cut on the Sorvall Porter Blum MT2-B ultramicrotome using dry glass knives. The knife angle was 10°. Ribbons of sections were transferred from the knife onto the surface of 50.0% v/v glycerol held in a Micromold® capsule, where the sections were allowed to stretch. The sections were then transferred to a coverslip by touching the coverslip to the surface of the glycerol. Prior to use the coverslips were cleaned for 15 minutes in chromic acid, rinsed in distilled water, air dried, covered with 0.1% w/v poly-L-lysine (MW 150,000-300,000, Sigma Chemical Co.) pH 8.5 for 10-15 minutes, rinsed in distilled water, and air dried (Wolesewick and De Mey, 1982). Most of the sections stuck to the coverslip in this way. The sections were immediately covered with pure glycerol and stored in a dust free place until staining took place.

The staining procedure was begun by rehydrating the sections. Since PEG is both water and ethanol soluble this also accomplished the removal of the PEG. Hydration was done by passing the coverslips through a descending concentration series of ethanol, 100%, 95%, two 70% changes, and 50%. Each change lasted 3 minutes, except the first 70% change which lasted 10 minutes and contained 1.0mg/ml of $NaBH_4$ to reduce background fluorescence (Weber et al., 1978). From the 50% ethanol the coverslips were passed into phosphate buffered saline (PBS) (8.0g NaCl, 0.2g KCl, 0.2g

KH_2PO_4, 1.15g Na_2HPO_4 per liter, pH 7.3) (Osborn and Weber, 1982), for 3 minutes. The coverslips were then placed in light tight boxes containing moist filter paper to maintain high humidity. The coverslips were flooded with PBS containing 1% w/v bovine serum albumin (BSA), type V (Sigma Chemical Co.), and placed in an incubator at 37°C. After 1 hour incubation the PBS-BSA was drained off, the sections covered with the appropriate dilution of the primary antibody, and the box placed in the incubator again at 37°C for 1-2 hours. This was followed by three 5-minute washes in PBS-BSA solution at room temperature. The last wash solution was drained off and replaced with the appropriate dilution of the secondary antibody and the box returned to the 37°C incubator for 45-60 minutes. This was followed by three 5 minute washes, with only PBS. The coverslips were then mounted onto glass slides. The mounting medium used reduces photobleaching with minimum quenching (Valnes and Brandtzaeg, 1985). It is made up by dissolving 1-2g of paraphenylenediamine (Fisher Scientific Co.) in a polyvinyl alcohol (PVA) solution. The PVA solution is made up by mixing 20.0g of solid PVA, type 11 (Sigma Chemical Co.) in 5.0ml of 1.0M Tris-HCl pH 9.0, 75.0ml of distilled water, and 10.0ml of glycerol (Valnes and Brandtzaeg, 1985). The preparations were viewed and photographed on a Zeiss Photomicroscope 11 equipped for epi-fluorescence.

The DGD embedding and sectioning procedure is a modification of prodedures used by Capco et al. (1984) and

Capco and McGaughey (1986). The DGD (MW 639.0) (Polysciences. Inc.) stock was kept molten in the oven at 55-60°C and 0.5% v/v of dimethylsulfoxide (DMSO) was added. The final change of 100% ethanol was first replaced with, a 2:1 mixture and then a 2:1 mixture of 100% ethanol and 1-butanol, followed by three changes of pure 1-butanol. These steps, 15 minutes each, were carried out at room temperature. A 2:1, followed by a 1:2, mixture of 1-butanol and DGD replaced the final pure 1-butanol change. These were done in the oven at 55-60°C and each one was of 1 hour duration. Infiltration was completed by two changes, 1 hour and overnight, of pure DGD at 55-60°C. Individual ovarioles were embedded in fresh DGD in Micromolds® and the DGD was then allowed to harden at room temperature.

The blocks were removed from the moulds and mounted onto wooden stubs with some molten DGD. Semi-thin (2.0μm) sections were cut on the Sorvall Porter Blum MT2-B ultramicrotome using glass knives fitted with water troughs. The knife angle was 10°. The sections were transferred from the trough to a coverslip with a fine wire loop attached to a piece of applicator stick. The coverslip was then warmed in the oven at 55-60°C until the sections had dried down, at which time the sections were immediately covered with pure glycerol. The coverslips had been cleaned and poly-L-lysine coated as described.

To remove the DGD from the sections, the coverslips were passed through three 1 hour changes of 1-butanol. The

coverslips were then brought through a series of transition fluids, composed of 7:3, 1:1, and 3:7 mixtures of 1-butanol and 100% ethanol, 3 minutes each, and finally into 95% ethanol. The staining procedure for DGD sections was identical to the PEG procedure from this point on.

Four different primary antibodies were used for immunofluorescence localizations. Two of these were rabbit polyclonal antibodies against sea urchin tubulin. One was a generous gift directly from Dr. K. Fujiwara, Harvard Medical School, and the second, prepared by his protocol, was purchased from Polysciences Inc.. These antibodies were used at a 1:50 to 1:100 dilution. The third primary antibody was a rabbit polyclonal antibody against Tetrahymena tubulin and the fourth one a mouse monoclonal antibody against Tetrahymena α- and β-tubulin. Both of these antibodies, originally prepared by Dr. J. Olmsted and Dr J. R. McIntosh respectively, were kindly supplied by Dr. G. Kidder, University of Western Ontario and were used at a 1:10 dilution. The secondary antibody used with the three polyclonal primary antibodies was a fluorescein conjugated goat anti-rabbit antibody (Miles-Yeda, Ltd.), at a 1:16 dilution. The secondary antibody used with the monoclonal primary antibody was a fluorescein conjugated goat anti-mouse antibody (Sigma Cemical Co.) at a 1:10 to 1:50 dilution.

Electrophoresis and electrophoretic transfer methods

For each stage examined between 200 and 280 desheathed ovarioles were homogenized in a buffer consisting of 25.0mM Tris-HCl pH 7.4, 1.0% v/v Nonidet P-40 (Sigma Chemical Co.), and 0.5% w/v sodium dodecyl sulfate (SDS) (TNS buffer) (based on Cleveland and Kirschner, 1982). To this buffer the following protease inhibitors were added: 1.0mM phenylmethyl-sulfonyl fluoride (PMSF), 1.0μg/ml pepstatin, 1.0μg/ml leupeptin, and 1.0μg/ml chemstatin. The ovarioles were homogenized in 100.0μl of TNS buffer. The homogenate was transferred to a 1.5ml polypropylene Eppendorf tube and the homogenizer was washed with additional 100.0μl of TNS buffer which was also added to the Eppendorf tube. The tube was next put in a sonicator water bath for 2 minutes and then spun at 10,000g for 10 minutes in an International Micro- Capillary Centrifuge, Model MB. The supernatant, from now on referred to as the sample, was collected. The protein concentration of the sample was determined by the method of Lowry et al. (1951). The sample was combined with an equal volume of electrophoresis sample buffer, 125.0mM Tris-HCl pH 6.8, 4.0% w/v SDS, 20.0% v/v glycerol, 10.0% v/v 2- mercaptoethanol, and 0.002% w/v bromophenol blue (Laemmli, 1970), and frozen at -70°C.

Polyacrylamide gel electrophoresis was carried out in the SDS-discontinuous system of Laemmli (1970), using a Protean 11 Cell (Bio-Rad laboratories) and LKB Bromma 2197 power supply. The Laemmli system allows for protein

separation based solely on molecular weight. The resolving gel (115.0mm x 160.0mm x 1.0mm) contained 10.0% w/v total acrylamide (Bio-Rad Laboratories), 2.7% w/w N, N'-methylene-bis-acrylamide (Bio-Rad Laboratories) as crosslinker (i. e. 10.0%T, 2.7%C), 375.0mM Tris-HCl pH 8.8, and 0.1% SDS. The gel was polymerized by the addition of ammonium persulfate (LKB-Produkter AB) and N, N, N', N'-tetramethylethylenediamine (TEMED) (LKB-Produkter AB) at final concentrations of 0.005% w/v and 0.03% v/v respectively. The stacking gel (20.0mm x 160.0mm x 1.0mm) contained 4.0%T, 2.7%C, 125.0mM Tris-HCl pH 6.8, and 0.1% w/v SDS, and was polymerized by 0.05% w/v ammonium persulfate and 0.05% v/v TEMED. The tank buffer was the same in both the upper and lower buffer chambers and consisted of 25.0mM Tris-HCl pH 8.3, 192.0mM glycine, and 0.1% w/v SDS. The upper buffer was discarded after use but the lower buffer was reused five times.

The samples were thawed shortly before a run, placed in a boiling water bath for 3 minutes, and spun at 10,000g for 10 minutes in an International Micro-Capillary Centrifuge, Model MB. The samples were loaded by a Hamilton microliter syringe (Hamilton Company Inc.) fitted with a piece of Intramedic polyethylene tubing (i. d. 0.58mm) (Clay Adams). The experimental samples were loaded at 50.0μg total protein per well. The gels and tank buffer were maintained at 10.0 °C during the run by circulating cooled water through the cooling core. The water was cooled and pumped by a Haake

FK-2 water circulator bath. Two gels were electrophoresed at a time and were run at a constant current of 20.0mamperes/gel until the tracking dye, bromophenol blue had reached a point about 1.0cm from the bottom of the gel.

Following electrophoresis the proteins were electrophoretically transferred from the resolving gel to a nitrocellulose (NC) sheet where they could be probed with anti-tubulin antibodies. The transfer procedure used was a modification of the original procedure by Towbin et al. (1979). The Bio-Rad Trans-Blot Cell and Bio-Rad Model 250/2.5 power supply were used for all transfers. The gel was first equilibrated for 30 minutes in transfer buffer, 25.0mM Tris pH 8.3, 192.0mM glycine, and 20.0% methanol. The gel and NC sheet, pre-wetted in transfer buffer, were sandwiched between four sheets of chromatography paper (Whatman #1) and two pieces of sponge pads in the gel holder, care being taken to expel all air bubbles from between the gel and the NC. The gel holder was inserted into the Trans-Blot Cell with the gel facing the cathode and the NC sheet facing the anode, and the chamber filled with transfer buffer with 0.1% w/v SDS added. This buffer was reused four or five times. The pre-chilled buffer was maintained at 5.0°C with the Haake FK-2 water circulator, and the transfer was done at a constant voltage of 70.0V, giving a field strength of 8.78V/cm, for 2 hours.

The gel was stained after completion of transfer to monitor the elution efficiency. Electrophoresis conditions

were monitored by also staining the gel not used for transfer. The gels were stained by a modified silver staining procedure (Morrissey, 1981). The gels were fixed overnight in 50.0% methanol followed by two 30 minute washes in distilled water and then soaked in 5.0μg/ml dithiothreitol (DTT) (Sigma Chemical Co.) for 30 minutes, and 0.1% w/v silver nitrate for additional 30 minutes after that. After this the gels were rinsed briefly, first in distilled water and then in developer (0.03g/ml anhydrous Na_2CO_3, 0.0185% v/v formaldehyde), and then soaked in developer. The reaction was stopped with 2.3M citric acid.

The NC sheets were stained either with amido black for total protein or with anti-tubulin antibody for the detection of tubulin. For staining of total protein the NC sheet was soaked in 0.1% w/v amido black in a 1:5:4 mixture of glacial acetic acid, methanol, and water for 5-10 minutes and then destained in three to four changes of a 2:90:8 mixture of glacial acetic acid, methanol, and water. Amido black staining was performed to assess the binding efficiency under a variety of transfer conditions.

The entire immunodetection procedure was done at room temperature with the NC membrane in a plastic freezer bag. The procedure was as follows: (1) the NC sheet was soaked for 15 minutes in Tris buffered saline containing 10.0mM Tris-HCl pH 8.8, 150.0mM NaCl, and 0.05% v/v polyoxyethelene-sorbitan monolaurate (Tween 20, Sigma Chemical Co.) (TBST); (2) an overnight incubation in 1.0%

w/v BSA in TBST; (3) the appropriate dilution of the primary antibody in BSA-TBST, incubated for 4-8 hours; (4) three 30 minute washes in TBST; (5) 4-8 hour incubation in the appropriate dilution of the alkaline phosphatase conjugated secondary antibody in BSA-TBST; (6) three 30 minute washes in TBST; (7) color development in alkaline phosphatase (AP) buffer (100.0mM Tris-HCl pH 9.9, 100.0mM NaCl, 5.0mM $MgCl_2$ with 0.33mg/ml of nitro blue tetrazolium (NBT) and 0.165mg/ml of 5-bromo-4-chloro-3-indolyl phosphate (BCIP). The color development was stopped in distilled water.

Two primary antibodies were used to stain NC sheets. One was the same monoclonal antibody, raised against Tetrahymena α- and β-tubulin, as used for immunofluorescence microscopy, but used here at a 1:100 dilution. The other primary antibody used was a mouse monoclonal antibody against slime mold β-tubulin. This antibody was generously supplied by Dr. E. Byard, University of Winnipeg and was used at a 1:500 dilution. The alkaline phosphatase conjugated secondary antibody used was a goat anti-mouse antibody and was used at a 1:7,500 dilution (Promega Biotec).

Bovine brain tubulin was used as a marker in gel electrophoresis and was isolated by the method of Borisy et al. (1975) as modified by Vallee et al. (1981). A once cycled MT pellet was obtained as a generous gift from Dr. E. Byard, University of Winnipeg. The MT pellet was resuspended in assembly buffer (0.1M PIPES pH 6.6, 0.1mM

ethylenediamine tetraacetic acid (EDTA), 1.0mM EGTA, 1.0mM $MgSO_4$, 1.0mM mercaptoethanol, and 1.0mM GTP) at 0-4°C and incubated at 0-4°C for 30 minutes. The preparation was then spun for 30 minutes at 4°C and 38,000g in a Beckman JA-20.1 rotor in a Beckman Model J2-21M Induction Drive Centrifuge. The supernatant was recovered and saved but the pellet was discarded. The supernatant was incubated at 37°C for 30 minutes and then centrifuged for 30 minutes at 37°C and 38,000g in the JA-20.1 rotor. The resultant pellet of twice cycled MT protein was used as reference protein in electrophoresis runs.

In addition to tubulin MW markers (LKB Bromma) were included in each run. These marker proteins included cytochrome c (MW 12,300), myoglobin (MW 17,200), carbonic anhydrase (MW 30,000), ovalbumin (MW 45,000), albumin (MW 66,250), and ovotransferrin (MW 77,000). The markers were used to construct a standard curve for the estimation of the MW of tubulin. The standard curve was obtained by plotting the Rf value for each protein, i. e. the distance from the top of the gel to the protein band divided by the distance from the top of the gel to the dye front, against $\log_{10}$ of its MW. The MW of tubulin was then determined by calculating its Rf value from stained gels, reading its $\log_{10}$ MW from the standard curve, and taking the antilog_{10} of this number.

Photography and photomicrography methods

Electron micrographs were taken on Kodak Electron Microscopic film 4489 and developed in a 1:2 dilution of Kodak D-19 developer. Polarizing micrographs were taken on Kodak Panatomic-X film (ISO 32), Kodak Tri-X Pan film (ISO 400), or Kodak Technical Pan film 2415 (ISO 200). These were developed in Acufine (Acufine, Inc.) according to manufacturer's specifications. Brightfield light micrographs were taken on Kodak Panatomic-X film at ISO 32 and developed as described. Immunofluorescence micrographs were taken on Kodak Tri-X Pan film at ISO 400 and developed as described above. Gels and NC sheets were photographed, while still wet, using Kodak Technical Pan film 2415 at ISO 25. This was developed in Acufine according to the specifications for Kodak Panatomic-X film. All film was printed on Ilford stabilization paper.

RESULTS

First results pertaining to methodological adaptations and evaluations will be presented. This will be followed by findings on the ontogeny of the MT arrays in the trophic core and cords.

Immunofluorescence methods

1. Fixations

Of the four fixatives evaluated, the 3.0% paraformaldehyde + 0.5% glutaraldehyde fixative gave the best results. This evaluation is based on good general morphological preservation, good preservation of tubulin antigenicity, and relatively low non-specific background fluorescence. Both the 1.0% paraformaldehyde and the 1.0% paraformaldehyde + 0.5% glutaraldehyde fixatives resulted in unsatisfactory morphological preservation (Figs. 1, 2). Good general morphological preservation was obtained with both the 3.0% paraformaldehyde + 0.1% glutaraldehyde and the 3.0% paraformaldehyde + 0.5% glutaraldehyde fixatives (Figs. 3, 4). The 3.0% paraformaldehyde + 0.5% glutarldehyde fixative was chosen for all subsequent fixations because glutaraldehyde is known to be an excellent preserver of antigenic determinants and the higher glutaraldehyde concentration did not impart any significant background

fluorescence to the tissue if a $NaBH_4$ reduction step was included in the staining procedure (Figs. 5, 6, 7).

2. Controls

Controls were included in order to verify the specificity of the anti-tubulin fluorescence staining. Removal of the embedding medium reveals background autofluorescence both due to preparative methods and the inherent fluorescence of the tissue. This kind of background was not a problem in this study (Figs. 5, 8). The background fluorescence imparted to the tissue by non-specific binding of the fluorescein conjugated secondary antibody was assessed by omitting the primary antibody. Instead the tissue was incubated with the secondary antibody directly after the PBS-BSA blocking step. Although the fluorescence intensity is fairly high in some of these preparations it is important to note that no specific pattern is observed (Figs. 6, 9). Confirmation of primary antibody specificity was further substantiated by observations of staining of known MT structures such as mitotic spindles (Figs. 10, 11) and the adult trophic core (Fig. 12).

3. Comparison of antibodies

No appreciable differences were observed in the fluorescence pattern produced with the four primary antibodies. The monoclonal anti-Tetrahymena tubulin

antibody gave the cleanest preparations with the least background staining. This antibody also resulted in the lowest fluorescence intensity of all four antibodies. This effect is however probably due to the secondary antibody rather than the primary antibody. The fluorescein/protein molar ratio for the anti-rabbit secondary antibody was 4.2 whereas the ratio for the anti-mouse secondary antibody was 3.3.

4. The use of PEG as an embedding medium

Two modification were made on the published PEG procedures. One modification was that the blocks were hardened at room temperature rather than in liquid nitrogen. This did not seem to have any adverse effects on the tissue, and was therefore adopted for the sake of simplicity.

The second modification involves the attachment of the sections to the coverslips. Initially, attempts were made at tacking the sections down onto the coverslip with a fine hair, and then warming the coverslip to 55°C (Wolosewick and De Mey, 1982). This resulted in such an unacceptably high level of folding and creasing of the sections that no usable results could be obtained. Relatively flat sections were obtained by placing a drop of distilled water on the coverslip, transferring the sections onto the drop and then evaporating the water off by warming the coverslip to 55°C. This however resulted in some sections staining only very weakly and others with only portions stained, apparently due

to loss of antigenicity upon air exposure. The method eventually adopted, i. e. flattening on 50.0% glycerol and then covering the sections with pure glycerol, gave relatively wrinkle free sections, bright fluorescence with low background, and there was no apparent loss of antigenicity, even after a storage period of up to one week (Figs. 5, 10, 11).

5. The use of DGD as an embedding medium

The use of DGD as an embedding medium for immunofluorescence microscopy of ovarioles required only one minor modification of the published DGD procedures. The infiltration times had to be lengthened because the original procedure was designed for tissue culture cells which, due to their small size, require only short infiltration times. With this modification in place, relatively wrinkle free and brightly staining sections with low background were easily obtained from DGD embedded tissue.

6. Comparison of PEG and DGD

PEG and DGD gave fluorescent images of equally good quality. The fluorescent pattern of MTs observed was the same for both media. DGD embedded tissue has slightly higher non-specific affinity for the fluorescein conjugated secondary antibody than PEG embedded tissue (Figs. 7, 9). While the embedding procedures take similar times for both media, the staining procedure is longer for DGD than PEG

material. This is because DGD is not ethanol miscible, and a series of transition fluids is therefore required. In addition it takes 3 hours to remove the DGD from the sections whereas the same operation takes no extra time for PEG because the PEG is solubilized in the hydration series. Wrinkle free sections are more easily obtained from DGD embedded tissue than PEG embedded tissue. This arises from the fact that DGD is not water soluble and DGD embedded tissue can therefore be sectioned onto water filled troughs. This minimizes compression of the tissue and also allows the sections to stretch on the water. A summary of these comparisons is in Table 1.

The development of MTs in the trophic core and cords

Microscopic observations

Polarizing microscopy observations were used to select the stages for examinination with the more involved immunofluorescence and TEM techniques. Hardly any birefringence could be discerned in ovarioles 8 dbm and 7 dbm (Figs. 13, 14). The first oocyte becomes visibly enlarged at 6 dbm and a narrow, faintly birefringent cord is seen connected to it (Fig. 15). By 5 dbm this cord has become quite bright in most ovarioles (Fig. 16). The anterior portion of the cord appears to lie within the presumptive trophic core (Fig. 16). It is very difficult, however, to accurately determine the division between cord and core in polarizing micrographs. It is also important to

note that considerable variation was observed at all stages (compare Fig. 16 and Fig. 17).

At 4 dbm there is still only one birefringent cord visible, but it has elongated and diffuse birefringence is also becoming visible in the larval core (Fig. 18). This pattern is also evident in immunofluorescence micrographs where, in longitudinal section, there are bright patches of fluorescence in nuclear-free areas (Fig. 19). In other areas of the presumptive core there is very little fluorescence (Fig. 20). Cross-sections through the oocyte area reveal bright fluorescence in the one larger cord connected to the growing oocyte and a number of small cords of the small oocytes (Fig. 21). An interesting feature in some of these small oocytes, and small oocytes at later stages, is perinuclear immunostained material (Fig. 21). The presumptive core area in cross-section appears as a number of discrete immunoreactive areas, i. e. more like a number of cords than a core (Fig. 22).

No major changes occur from 4 dbm to 3 dbm. Polarizing microscopy shows that the single large cord has thickened and lengthened (Fig. 23). Immunofluorescence micrographs show that in some ovarioles a second cord has become prominent with an increase in tubulin staining (Figs. 24, 25). One, and sometimes two larger immunostained cords and numerous small immunostained cords are seen in cross-sections through the posterior tropharium (Fig. 26). The larval core still has large areas with little if any staining (Figs. 24, 27, 28).

All 2 dbm ovarioles have at least one large cord containing MTs (Figs. 29, 30) and in many the second MT containing cord has grown almost to the same size as the first (Fig. 32). The future core has larger fluorescent areas than before (Figs. 31, 33) even though non-fluorescent core-like areas are still frequently encountered (Fig. 34). This is also evident from electron micrographs where larval core areas (Fig. 35) are occupied by extensive membrane systems with open, nucleus-free, cytoplasmic areas in between (Figs. 36, 37). Some of these areas have only a few, non-aligned MTs (Fig. 38), whereas others have a relatively high density of longitudinally arranged MTs (Fig. 39). Cross-sections through the oocyte area (Fig. 40) reveal that large cords have a much higher MT density than do small cords (Figs. 41, 42).

Two prominent cords with MTs have invariably developed by 1 dbm (Figs. 43, 44, 45). Polarizing micrographs frequently give the impression the cords fuse, thus forming a core (Fig. 43). The fact that no adult-like core is seen in immunofluorescence micrographs indicates however that this is due to superimposition (Fig. 46). There are still extensive presumtive core areas with only very scant immunoreactive material (Figs.44,46).

A third large MT containing cord appears in some ovarioles by 0 dpm (Fig. 47). Most ovarioles, however, have only two large cords at this stage (Figs. 48, 49). The first signs of an adult-like core are observed at this

stage, the definition of an adult-core being that it is a common area into which two or more cords connect. In some cases this appears to arise from the fusion of cords (Fig. 47), whereas in others it appears more as a flairing out or expansion of the anterior end of a large cord (Fig. 48). In most cases though, much of the core is still larval-like, with the immunoreactive material restricted to cord-like patches and other nucleus-free areas devoid of fluorescence (Figs. 50, 51). The core (Fig. 52) has MTs arranged both longitudinally (Fig. 54) and perpendicular to the long axis of the ovariole (Fig. 53). Cords (Fig. 55) have MTs occasionally arranged perpendicular to the long axis of the ovariole (Fig. 56) but the MTs most frequently are arranged longitudinally (Figs. 57, 58).

By 1 dpm there are still two to three large MT packed cords present (Figs. 59, 60, 61, 67, 68, 69). The proportion of ovarioles with three large cords has increased from 0 dpm. All ovarioles have an adult core by this stage and this core shows more fusion of the immunostained cord-like patches than before (Figs. 60, 62). Other core areas which lack discrete bright immunostained patches show fainter more diffuse staining (Fig. 63). The ultrastructure of the core (Figs. 64, 65, 66) and the large cords (Fig. 67, 68, 69) remains essentially unchanged from 0 dpm, i. e. majority of the MTs are arranged longitudinally.

No major changes were apparent between 1 dpm and 2 dpm. One massive MT containing cord and one or two other large MT

containing cords are present (Figs. 70, 71, 72, 77, 79). In many cases these still appear to extend into the posterior presumptive core as separate and discrete cord-like structures (Figs. 71, 72, 73). In the anterior presumtive core these sometimes flair out, forming areas of fainter more diffuse anti-tubulin staining (Figs. 71, 72, 74). The anterior core however still has separate cord-like structures (Figs. 72, 74). Ultrastructurally, the core (Fig. 75) has large areas with a high density of longitudinally arranged MTs (Fig. 76). There are other membrane and nucleus-free areas also which have only few MTs (Fig. 77) and still other areas which have a very extensive and tortuous membrane system (Fig. 78). TEM reveals a somewhat higher density of MTs in large cords (Figs. 79, 81) than in smaller cords (Fig. 80).

There is a gradual increase in MT density in the presumtive core from 2 dbm to 2 dpm (Table 2). The density increases from 24.9 MTs/μm^2 on 2 dbm to 41.2 MTs/μm^2 on 2 dpm.

Biochemical observations

Anti-tubulin staining of electrophoretically separated and transferred ovarian proteins reveals a gradual increase in the relative amount of tubulin from 6 dbm to 1 dbm (Figs. 82, 83). Essentially the same pattern was observed with the antibody against slime mold β-tubulin (Fig. 82) and the antibody against Tetrahymena α- and β-tubulin (Fig. 83),

except that the results with the latter indicate a decrease in tubulin levels between 3 dbm and 1 dbm. Two other minor differences were observed between the two antibodies. One is that the former antibody stains brain tubulin fainter and the ovarian tubulin more intense as compared to the latter antibody (Figs. 82, 83). The other difference is that even though a number of non-tubulin bands stain faintly with both antibodies, this effect is less pronounced with the anti-Tetrahymena antibody (Figs. 82, 83).

Bovine brain tubulin and ovarian tubulin migrated at the same rate under the electrophoresis conditions used in this study. The MW of tubulin was about 52,000.

Silver staining of gels after transfer confirms that under the transfer conditions used, only some of the high MW proteins remain in the gel (Fig. 84). Control staining of the NC membrane, i. e. staining according to the described protocol but with the primary antibody omitted, shows that general background staining was not a problem in this study, and that the non-tubulin band stained in the regular staining procedure are the result of non-specific primary antibody binding (Fig. 85).

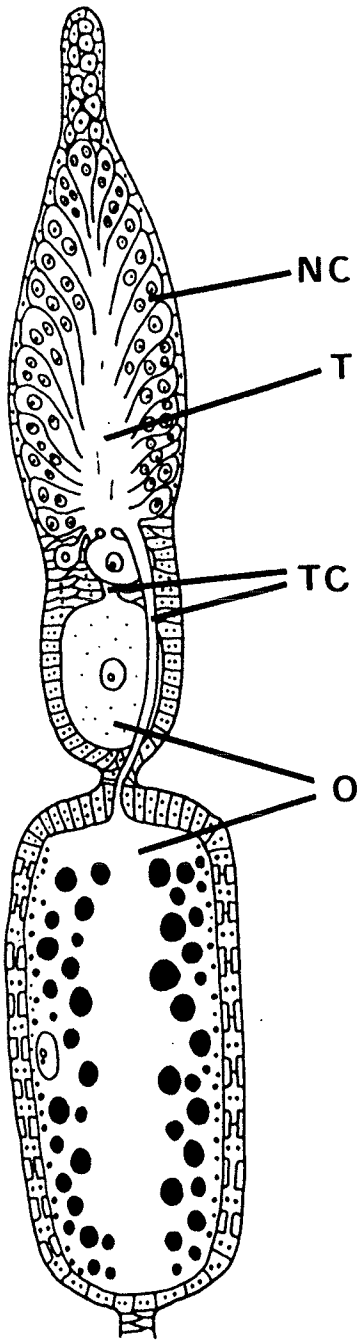

Diagram 1. Summary diagram of the adult Rhodnius ovariole. Nurse cells (NC), oocytes (O), triphic core (T), trophic cords (TC), (based on Huebner, 1984b).

TABLE 1

Comparison of PEG and DGD

	PEG	DGD
Embedding time	4 hours and an overnight infiltration step.	4 hours and an overnight infiltration step.
Staining time	4 hours.	7 hours.
Sectioning.	Easy to section. Folding of sections a common problem.	Easy to section. Folding of sections only a minor problem.
Background fluorescence.	Low autofluorescence and low non-specific fluorescence.	Low autofluorescence but higher non-specific fluorescence.
Fluorescence image.	Excellent.	Excellent.

TABLE 2

Stage specific MT packing in the presumtive and early adult trophic core (MTs/μm^2)

Stage	2 dbm	0 dpm	1 dpm	2 dpm
MT packing.	24±13.5	26.1±4.5	30.6±17.2	41.2±5.1

Figure abbreviations

M	Mitochondrion
MF	Microfilaments
MS	Mitotic spindle
MT	Microtubules
NC	Nurse cell
O	Oocyte
PNC	Perinuclear circle
PT	Presumptive or larval core
T	Adult trophic core
TC	Trophic cord

Figures

Plate 1.

Fixative assessment and immunofluorescence controls.

Figures 1-4. These toluidine blue stained brightfield micrographs illustrate the general morphology of the ovariole using various fixatives. Note the extensive extraction with 1% paraformaldehyde (Fig. 1) and to a lesser extent with 1% paraformaldehyde + 0.5% glutaraldehyde (Fig. 2). Both 3% paraformaldehyde + 0.1% glutaraldehyde (Fig. 3) and 3% paraformaldehyde + 0.5% glutaraldehyde (Fig. 4) result in good morphological preservation of the tissue. X200, X550, X600, X550.

Figure 5. The neglegible autofluorescence of PEG embedded tissue is revealed after removal of the PEG and $NaBH_4$ treatment. X550.

Figures 6-7. These figures illustrate PEG sections incubated in PBS-BSA (1 hour) followed by fluorescein conjugated secondary antibody (1 hour). Reduction of background fluorescence after $NaBH_4$ treatment is evident in Fig. 6 when compared to non-treatment (Fig. 7).

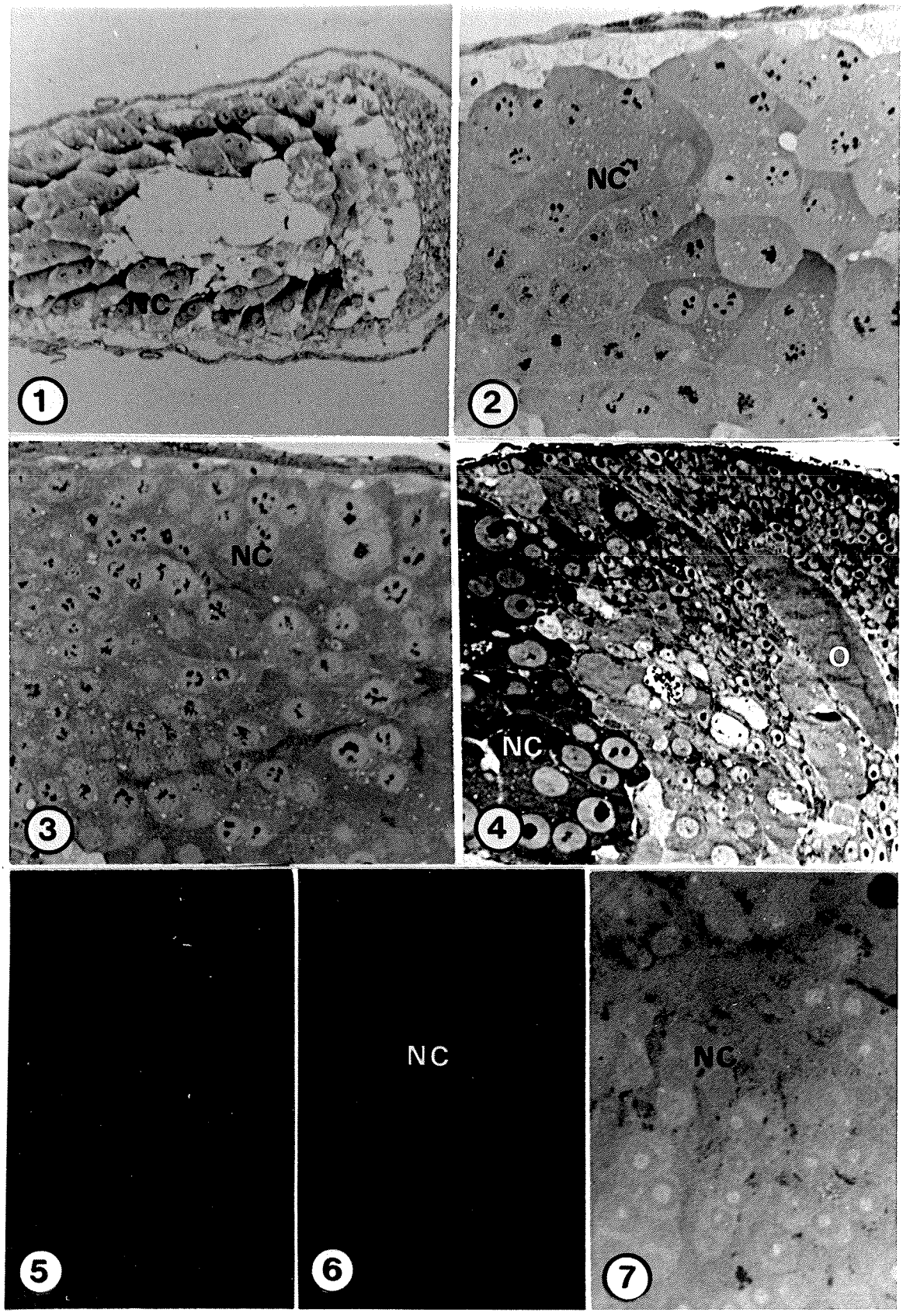
NC
1
NC
2
NC
3
O
NC
4
5
NC
6
NC
7

Plate 2.

Immunofluorescence controls.

Figures 8-9. DGD embedded controls. Note the low level of autofluorescence (Fig. 8), and the non-specific background fluorescence (Fig. 9). X400, X750.

Figures 10-12. The specificity of the primary antibodies was confirmed by the specific staining of mitotic spindles (Figs. 10, 11) and the adult trophic core and cords (Fig. 12). X1700, X600, X750.

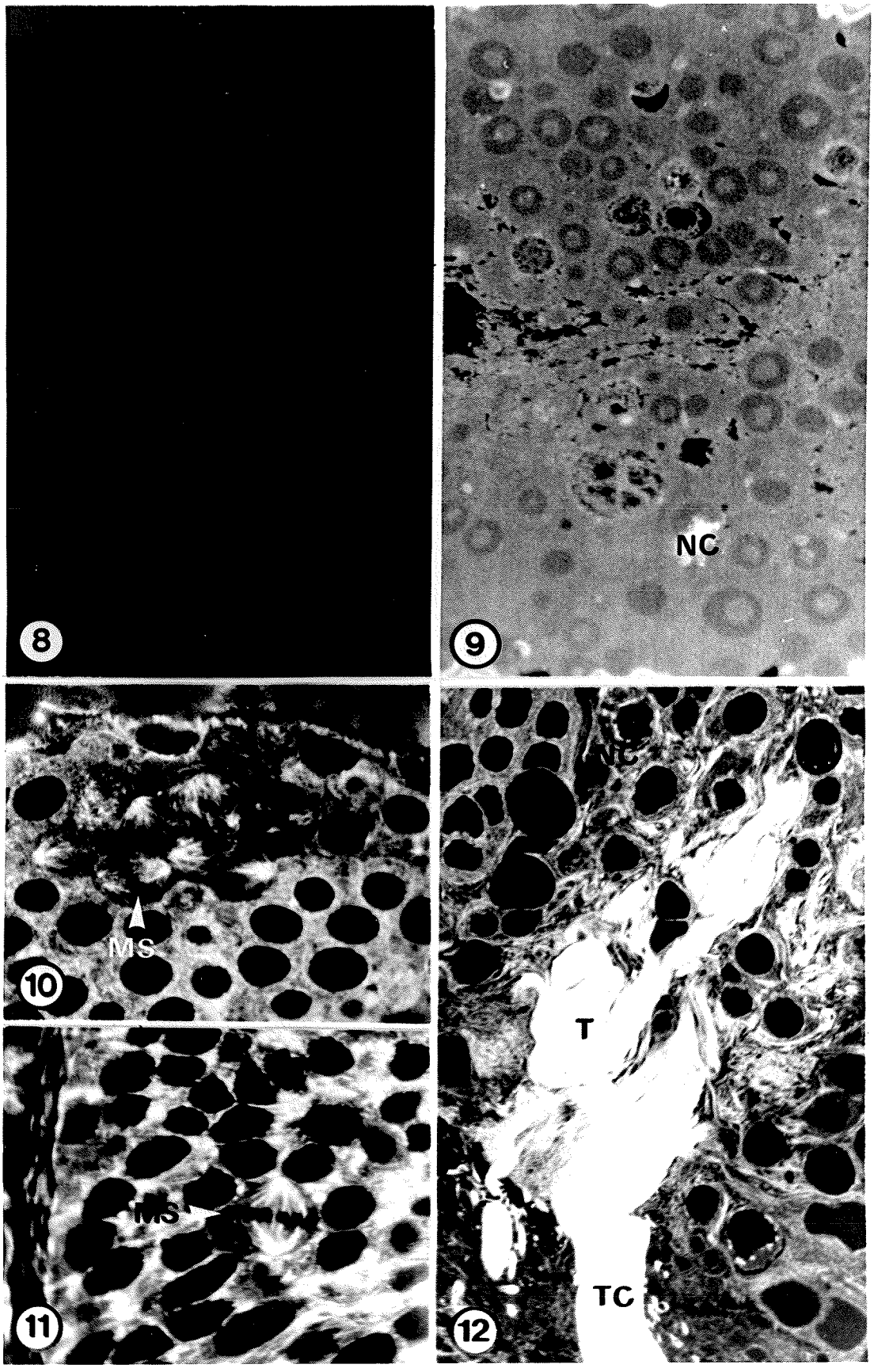
8
NC
9
MS
10
MS
11
NC
T
TC
12

Plate 3.

The earliest appearance of MTs.

Figures 13-14. These polarizing micrographs reveal neglegible birefringence in 8 dbm (Fig. 13) and 7 dbm (Fig. 14) ovarioles. X150, X250.

Figure 15. Polarizing micrograph of a 6 dbm ovariole showing the first appearance of a birefringent trophic cord. Note that an oocyte has begun to grow. X250.

Figures 16-17. Polarizing micrographs of 5 dbm ovarioles. Most ovarioles have developed one large birefringent trophic cord at this stage and some birefringence is present in the presumtive core (Fig. 16). Other ovarioles are less advanced (Fig. 17). X150, X150.

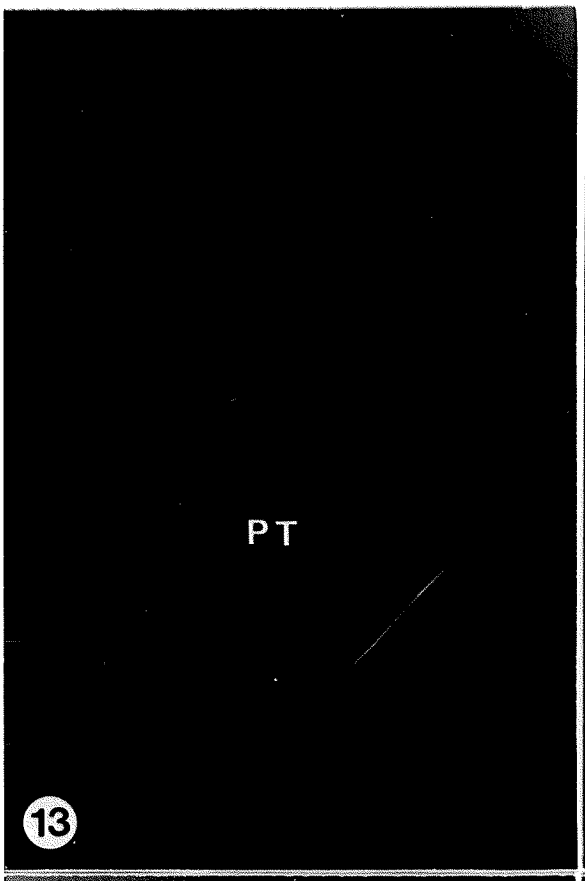
PT
13

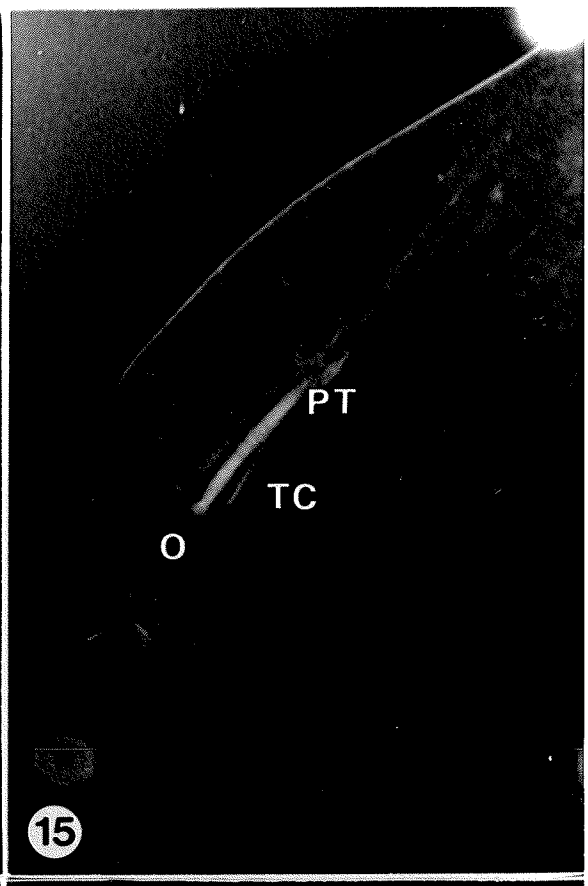
PT
TC
O
15

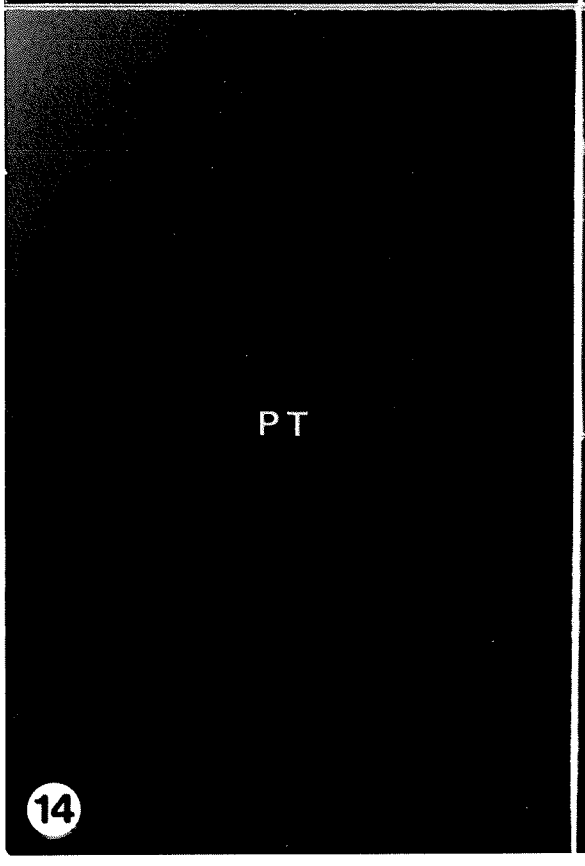
PT
14

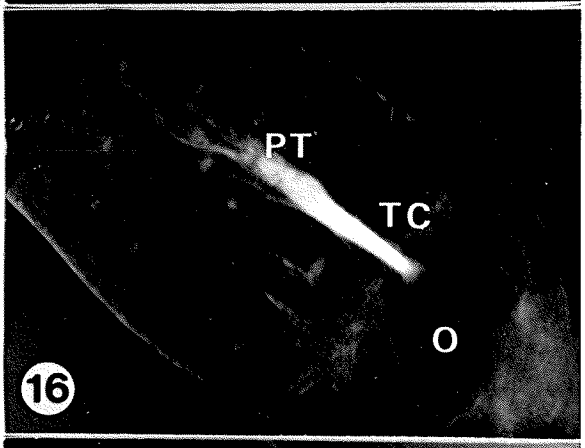
PT
TC
O
16

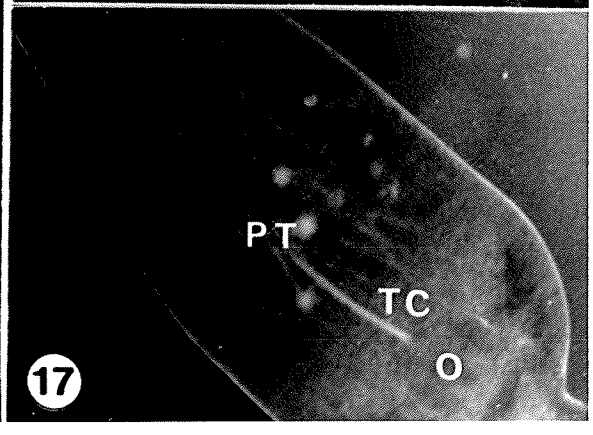
PT
TC
O
17

Plate 4.

4 days before molt.

Figure 18. Polarizing micrograph showing a birefringent trophic cord and increasing birefringence in the presumptive trophic core. X150.

Figures 19-20. Immunofluorescence micrographs, longitudinal sections, PEG embedding, revealing that some areas of the presumptive core are occupied by MTs (Fig. 19) while other areas are devoid of MTs (Fig. 20). X650, X500.

Figure 21. This immunofluorescence micrograph, PEG embedding, oblique section through the oocyte area, shows a single large, MT packed, trophic cord and numerous small MT containing cords (arrows). Note the perinuclear circle of MTs in small oocytes. X500.

Figure 22. This immunofluorescence micrograph, cross section, PEG embedding, illustrates that the MT staining of the posterior presumptive core resembles that of the trophic cords in Fig. 21. X650.

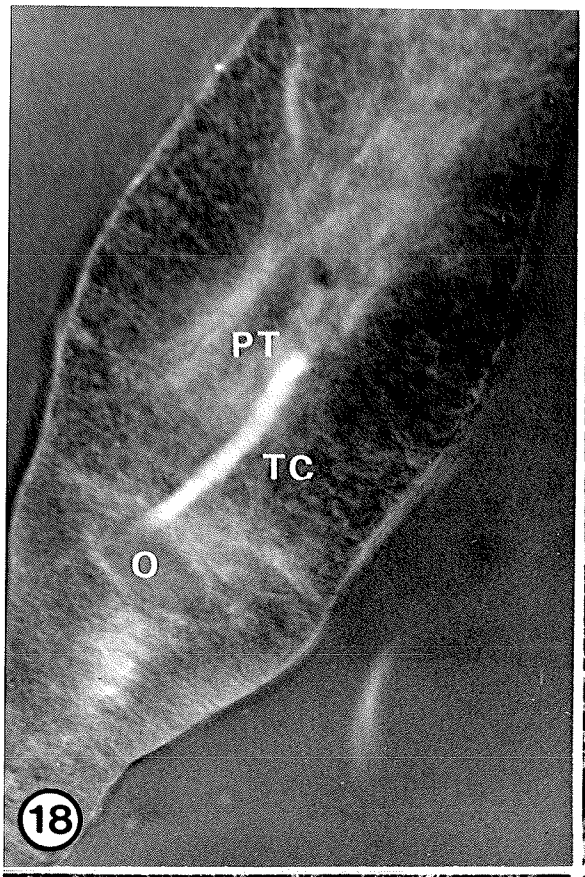
PT
TC
O
18

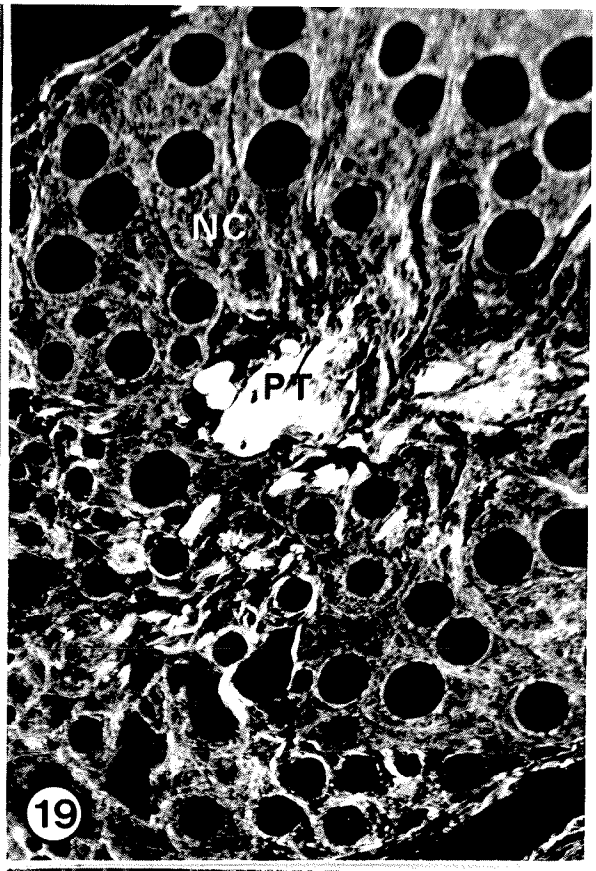
NC
PT
19

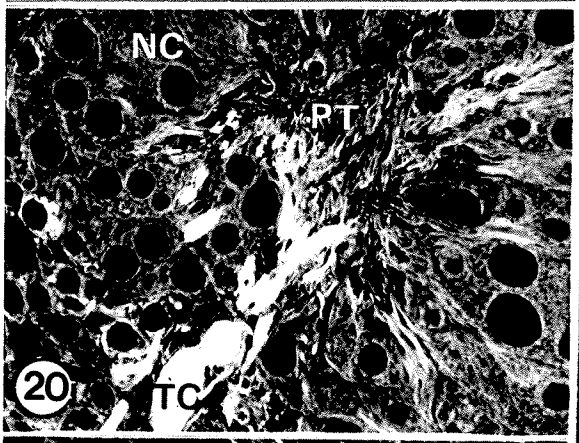
NC
PT
20
TC

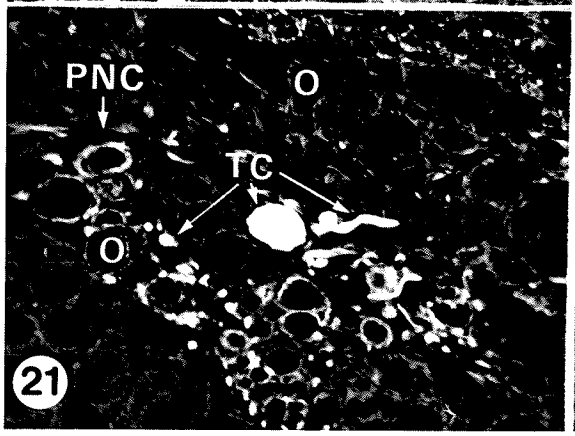
PNC
O
TC
O
21

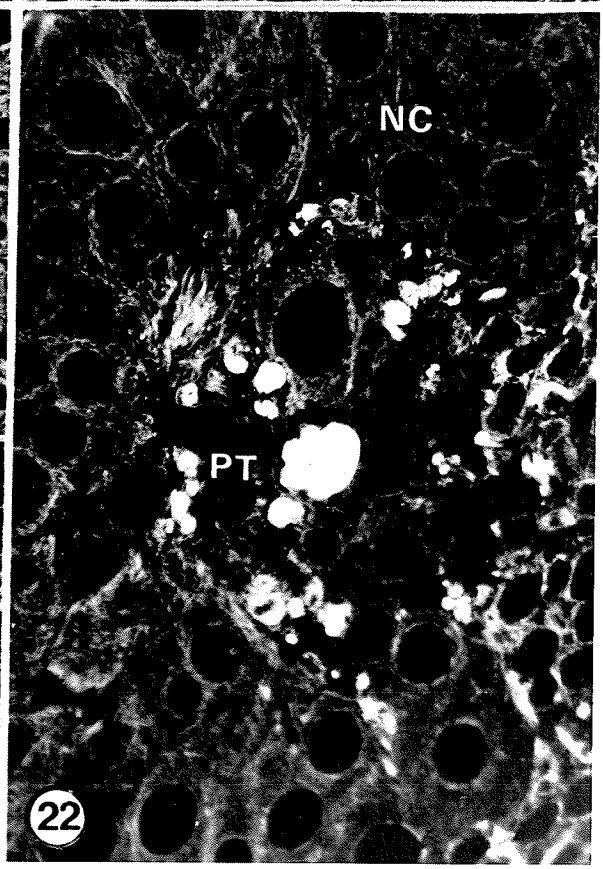
NC
PT
22

Plate 5.

3 days before molt.

Figure 23. This polarizing micrograph illustrates an enlarged trophic cord connected to an oocyte. X150.

Figures 24-25. These immunofluorescence micrographs, longitudinal sections, PEG embedding, reveal the patchiness of MT staining in the presumptive core (Fig. 24) and two MT containing cords (Fig. 25). X450, X550.

Figures 26-28. Numerous small MT containing cords in the oocyte area (Fig. 26) and the uneven distribution of MTs in the posterior (Fig. 27) and anterior (Fig. 28) presumptive core are shown in these immunofluorescence micrographs, cross sections, PEG embedding. X600, X750, X600.

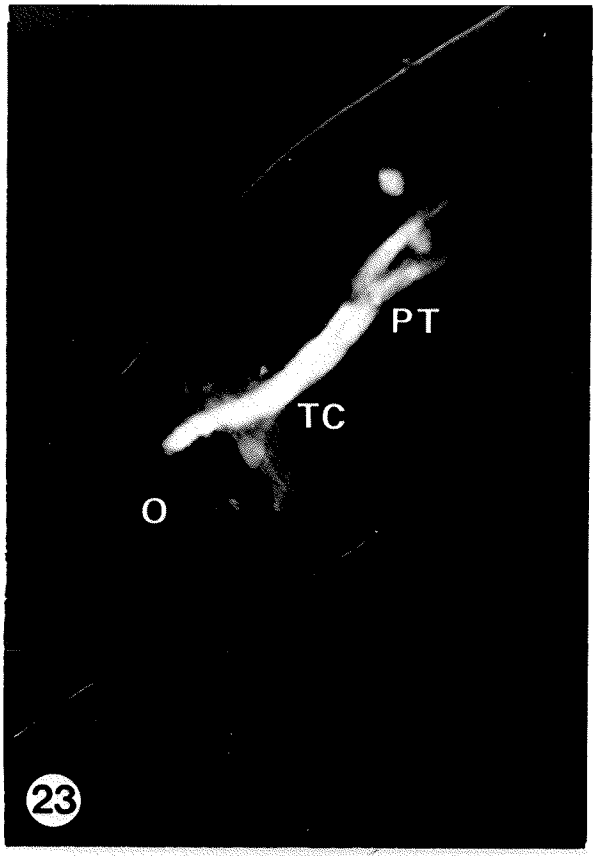
PT
TC
O
23

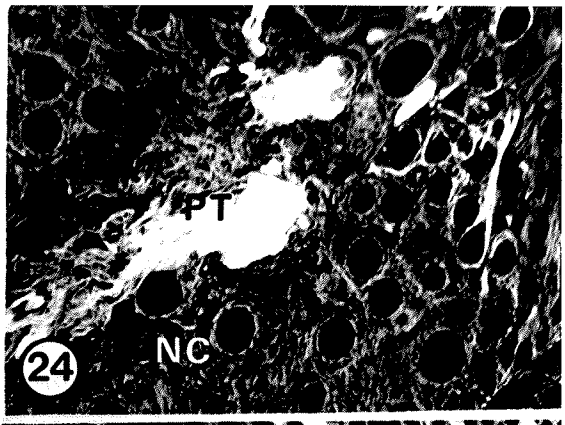
PT
NC
24

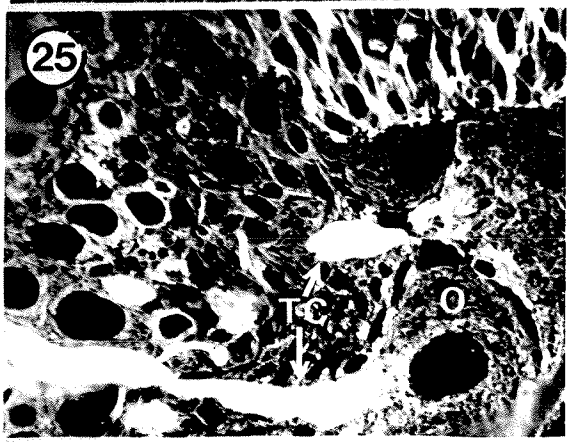
25
TC
O

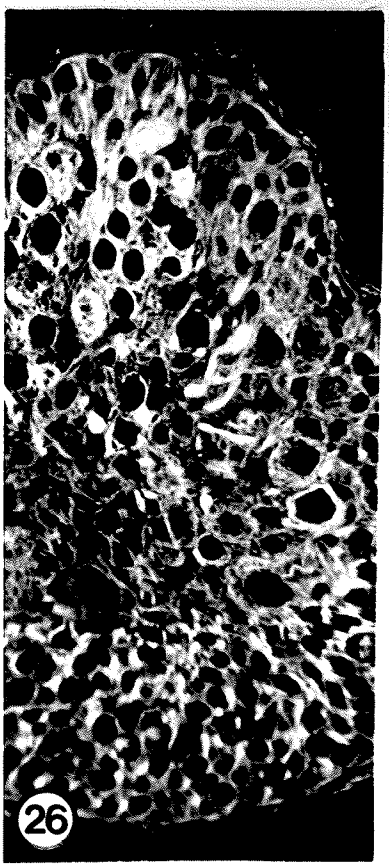
26

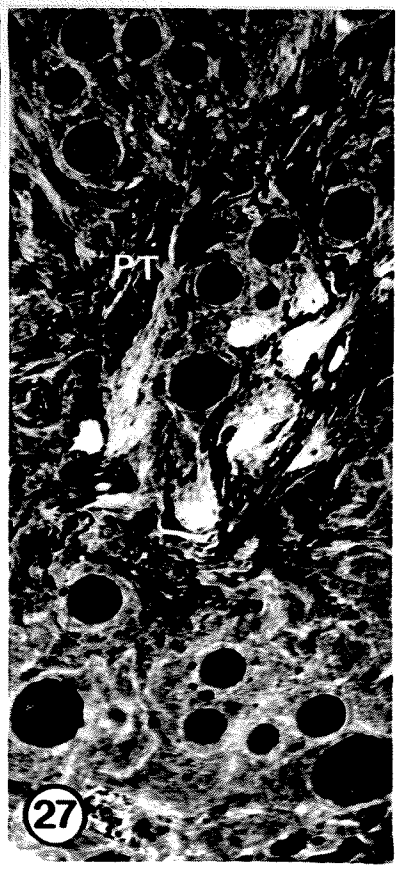
PT
27

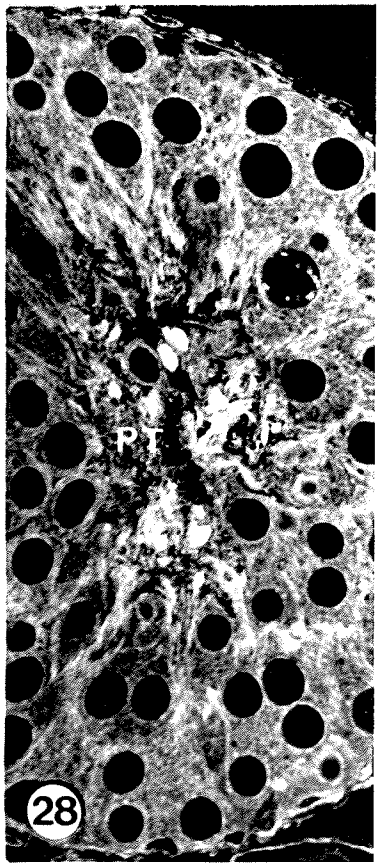
PT
28

Plate 6.

2 days before molt.

Figure 29. Polarizing micrograph showing a large trophic cord. Note that the anterior portion of the cord extends into the presumtive core area. X150.

Figure 30. A large trophic cord is seen extending into the posterior presumptive core in this immunofluorescence micrograph, longitudinal section, PEG embedding. X500.

Figure 31. This immunofluorescence micrograph, PEG embedding, longitudinal section, illustrates that the presumptive core has an uneven MT distribution. X500.

Figure 32. Immunofluorescence micrograph, PEG embedding, oblique section through the oocyte area. Note two large trophic cords (arrowheads) and numerous small trophic cords. X400.

Figures 33-34. Immunofluorescence micrographs, PEG embedding, cross sections through the presumptive core. X900, X600.

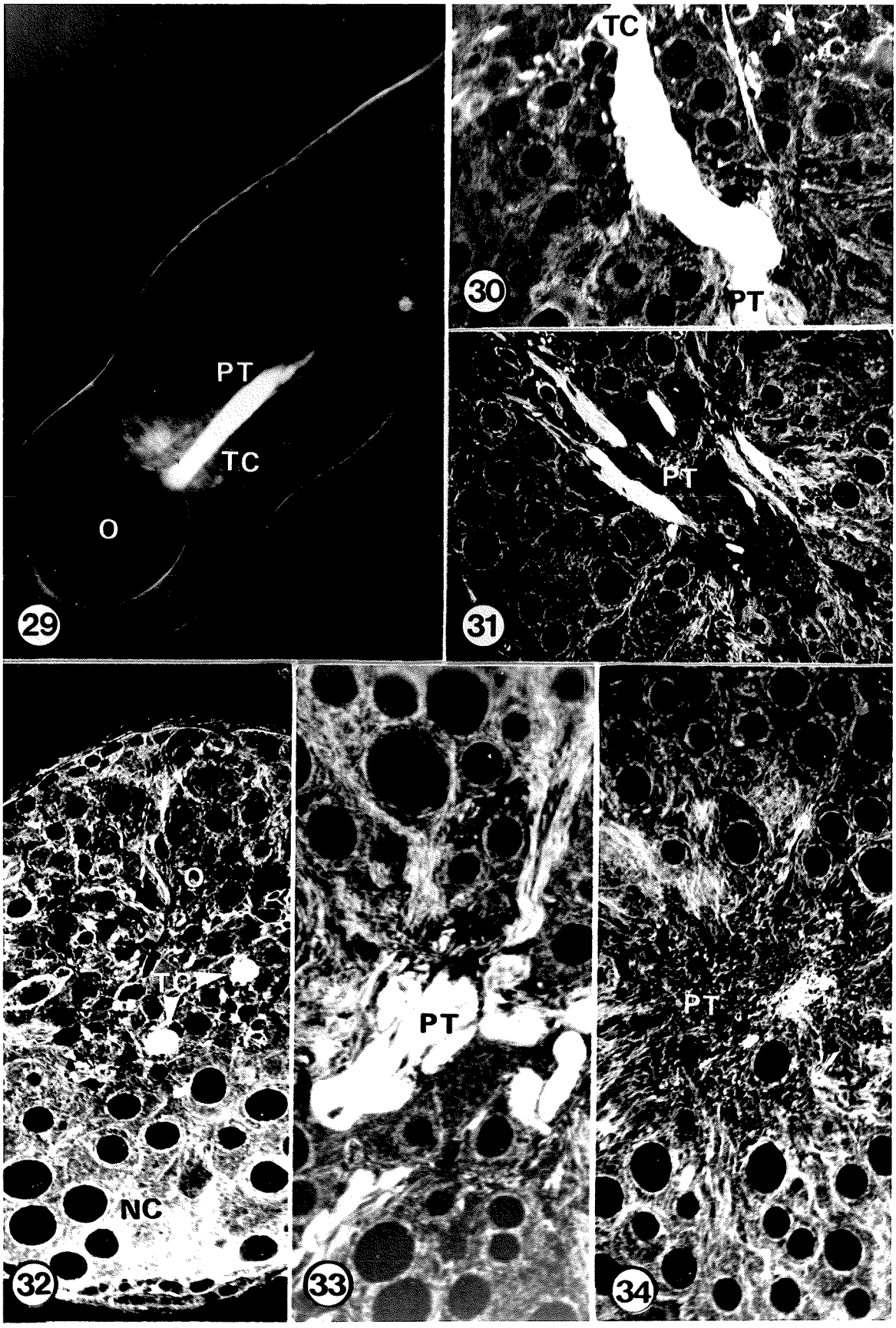
PT
TC
O
29
TC
PT
30
PT
31
O
TC
NC
32
PT
33
PT
34

Plate 7.

2 days before molt.

Figure 35. This brightfield micrograph illustrates the presumptive core area corresponding to the areas in Figs. 36-39. X300.

Figures 36-37. Note the complex nature, extensive membranes interspersed with open areas, of the presumptive core in these TEMs. X13,000, X11,500.

Figures 38-39. These TEMs, cross sections through the presumptive core, reveal a few MTs (arrows) in some of the open areas (Fig. 38) while other areas (Fig. 39) have numerous longitudinal MTs (arrows). X35,500, X74,500.

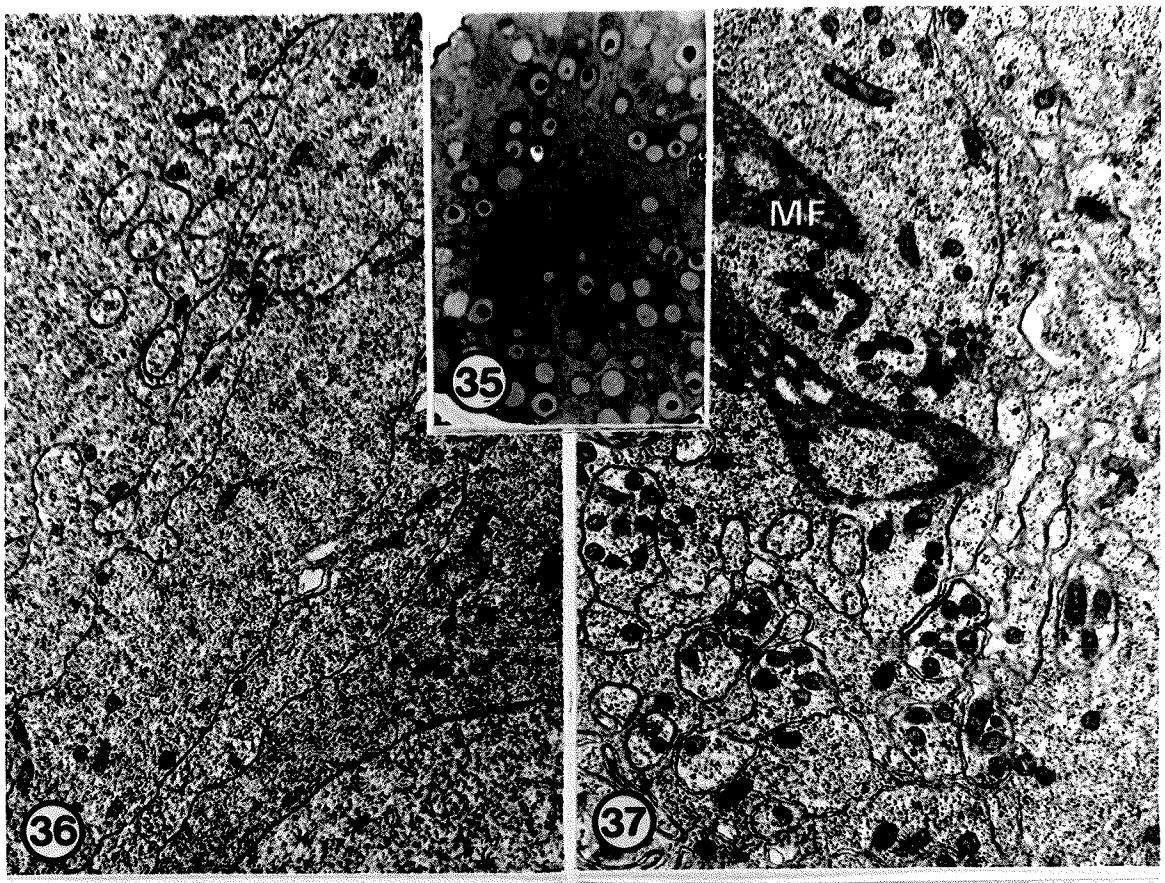
35
MF
36
37

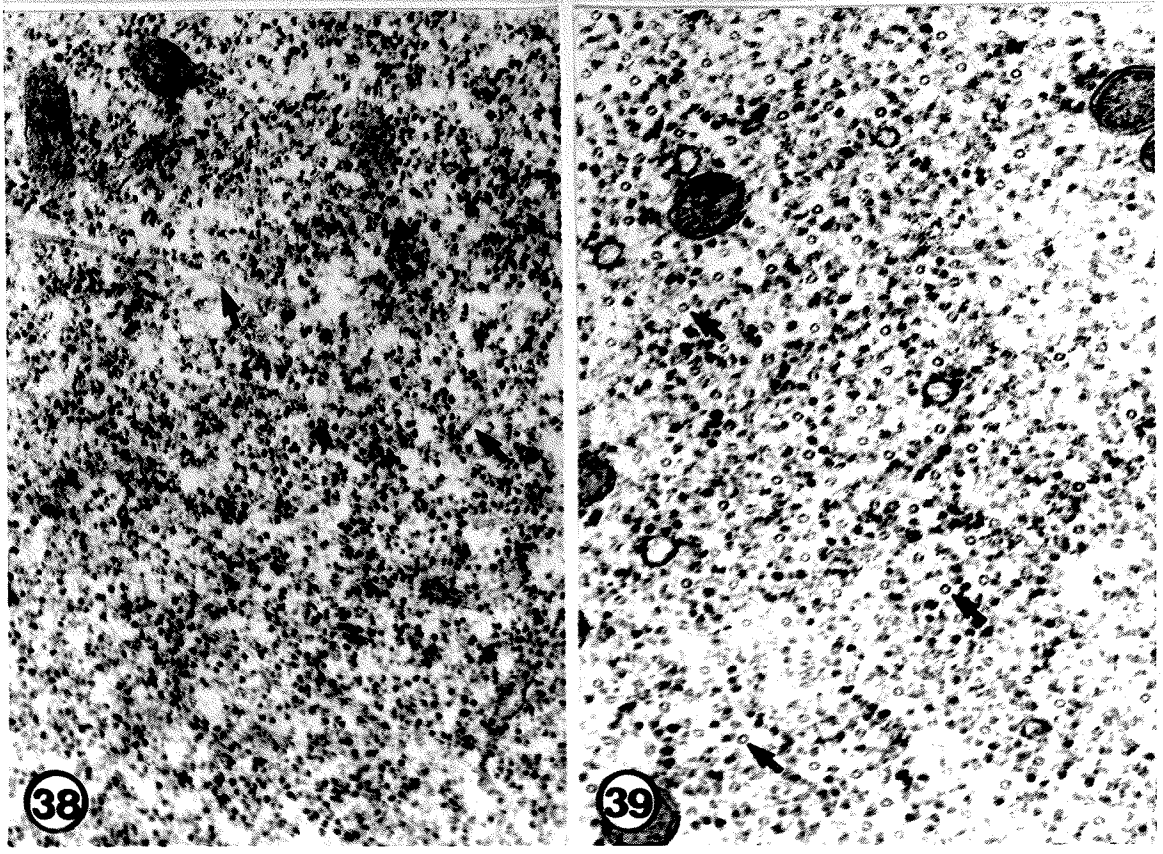
38
39

Plate 8.

2 days before molt.

Figure 40. Brightfield micrograph showing numerous small oocytes and small trophic cords, cross section. X600.

Figures 41-42. These TEMs reveal the increased MT packing density in growing cords (Fig. 41) as compared with non-growing cords (Fig. 42). X46,500, X47,000.

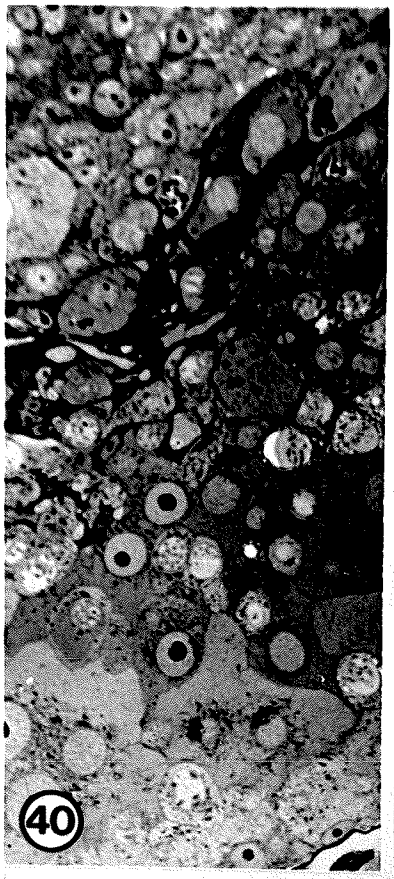

40

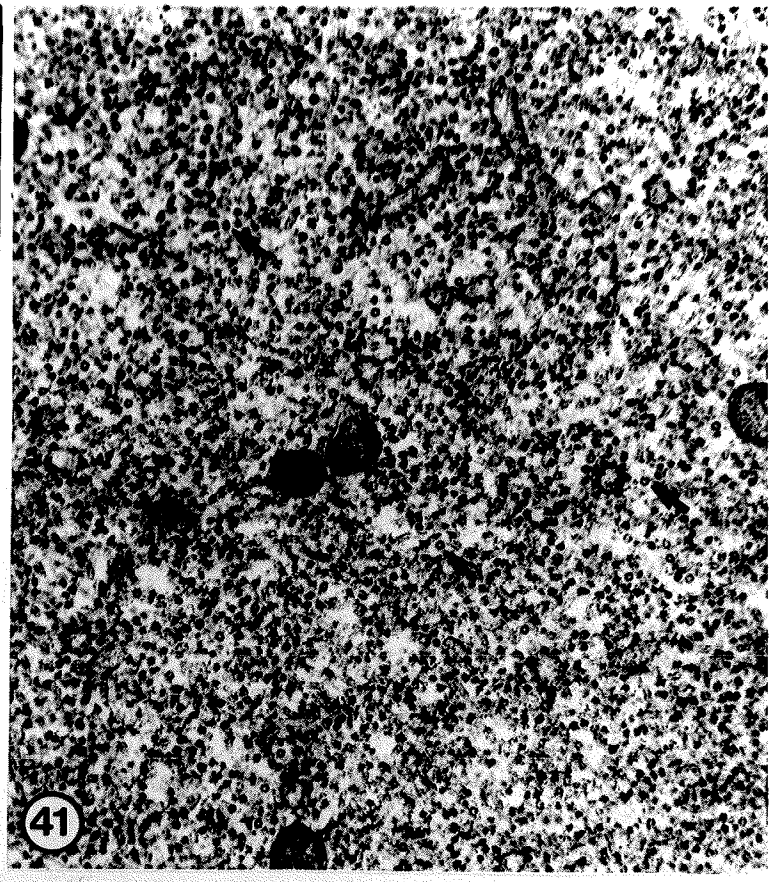

41

42

Plate 9.

1 day before molt.

Figure 43. A polarizing micrograph showing birefringence in two trophic cords and in the presumptive core. X150.

Figure 44. This immunofluorescence micrograph, longitudinal section, PEG embedding, illustrates two large, MT packed, trophic cords (arrows) and the presumptive core. X650.

Figures 45-46. These immunofluorescence micrographs, cross sections, PEG embedding, reveal two large cords and numerous small cords (arrows) in the oocyte area (Fig. 45) and the presumptive core (Fig. 46). X850, X600.

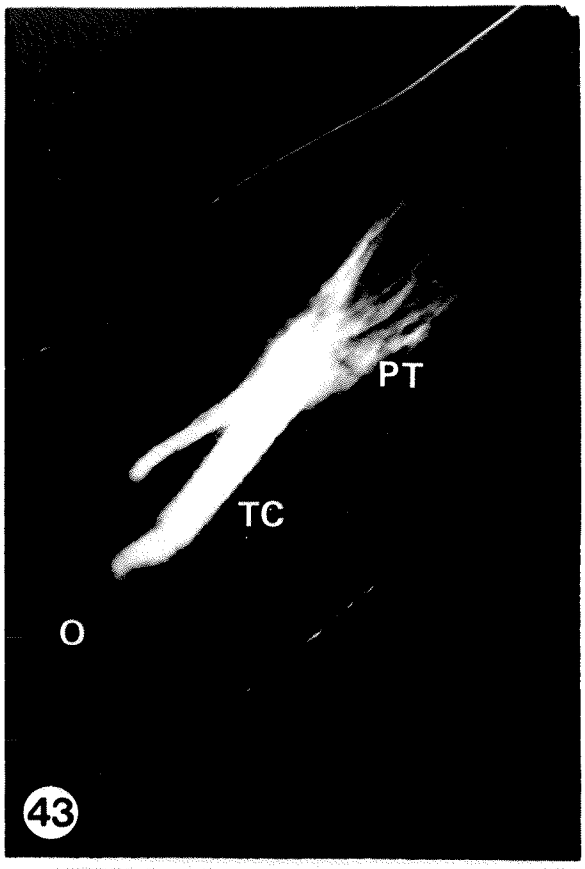
PT
TC
O
43

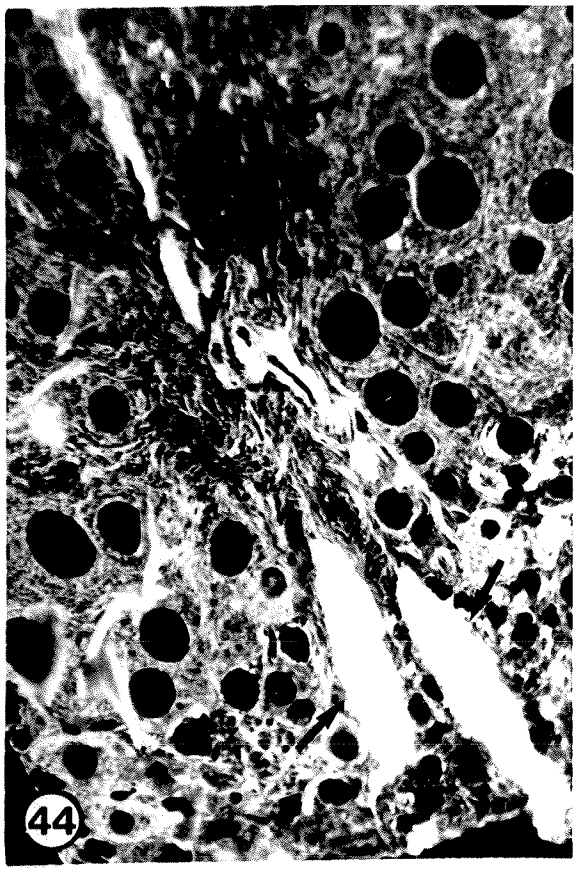
44

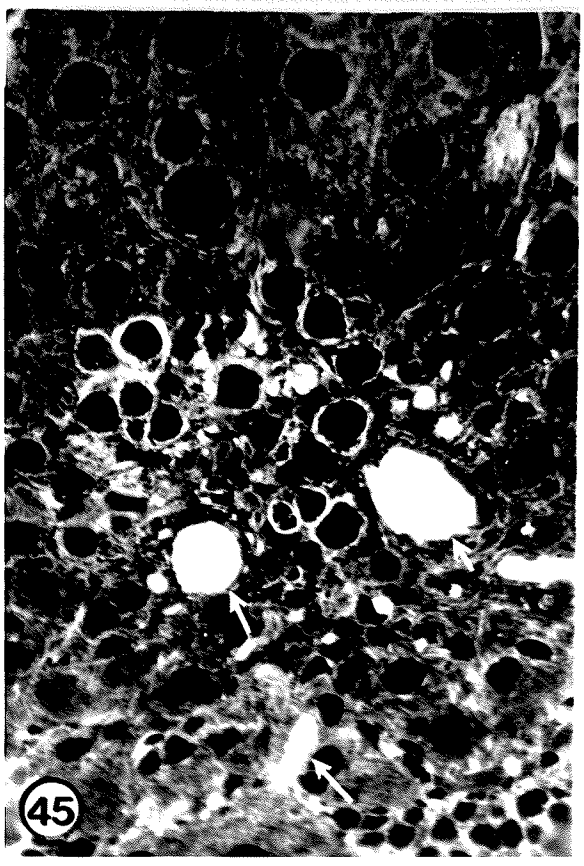
45

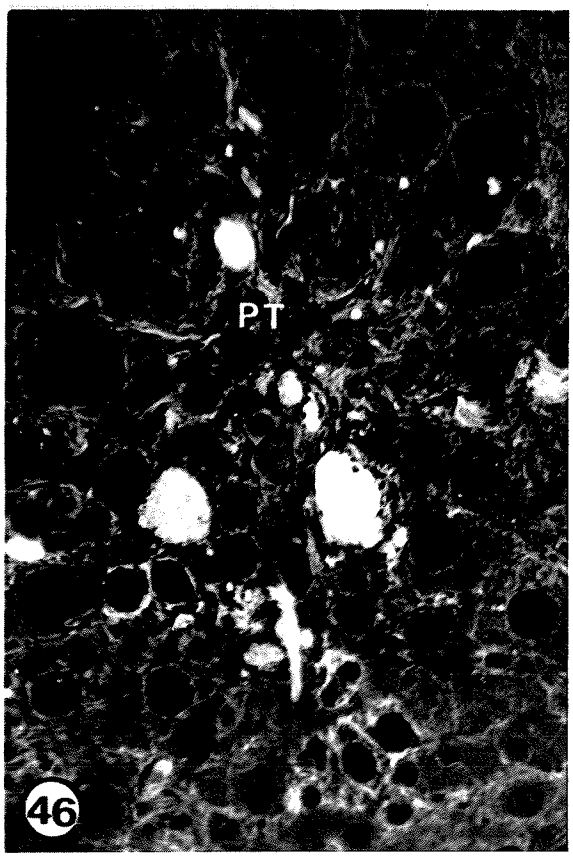
PT
46

Plate 10.

0 day post molt.

Figure 47. This polarizing micrograph shows three birefringent trophic cords and the first sign of an early adult core. X150.

Figure 48. An immunofluorescence micrograph, longitudinal section, PEG embedding, illustrating two trophic cords and the early adult core. X700.

Figures 49-51. These immunofluorescence micrographs, cross sections, PEG embedding, show large and small trophic cords (arrows) in the oocyte area (Fig. 49) as well as the variable appearance of the early adult core (Figs. 50, 51). X700, X600, X550.

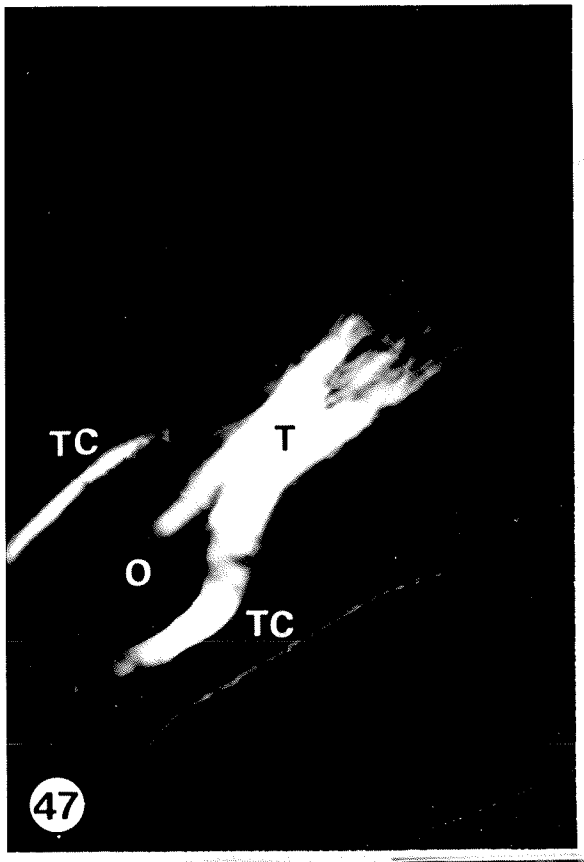
TC
T
O
TC
47


T
48
TC

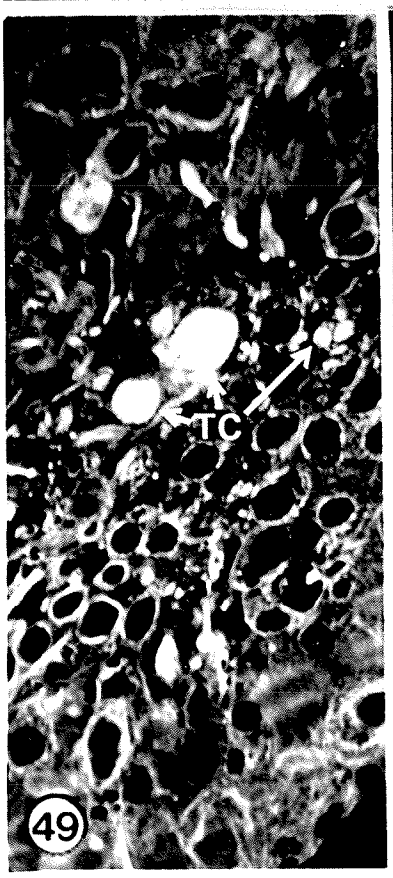
TC
49


T
50

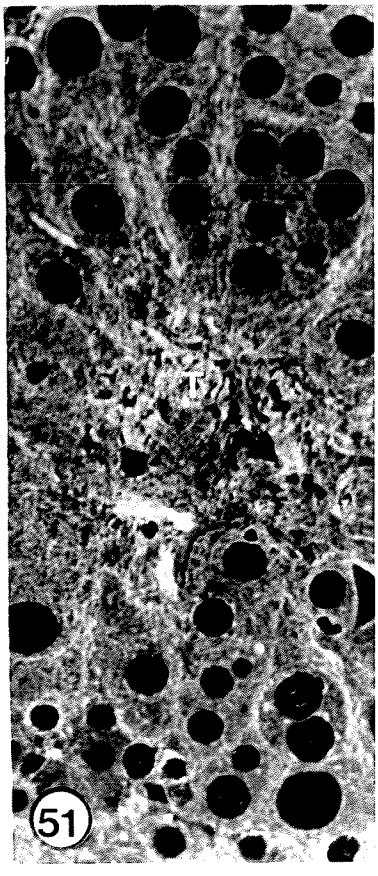
T
51

Plate 11.

0 day post molt.

Figure 52. This brightfield micrograph, cross section, illustrates the early adult core area adjacent to the areas in Figs. 53-54. X500.

Figures 53-54 These TEMs show that the early adult core has MTs (arrows) arranged longitudinally (Fig. 53) and perpendicularly (Fig. 54). X51,000, X52,000.

Figure 55. A brightfield micrograph, cross section through the posterior oocyte area, showing growing oocytes and trophic cords. X450.

Figures 56-58. These TEMs, cross sections through growing cords, illustrate a perpendicular arrangement of MTs (arrows) (Fig. 56) and the more common longitudinal arrangement (Figs. 57, 58). X60,000, X38,000, X50,000.

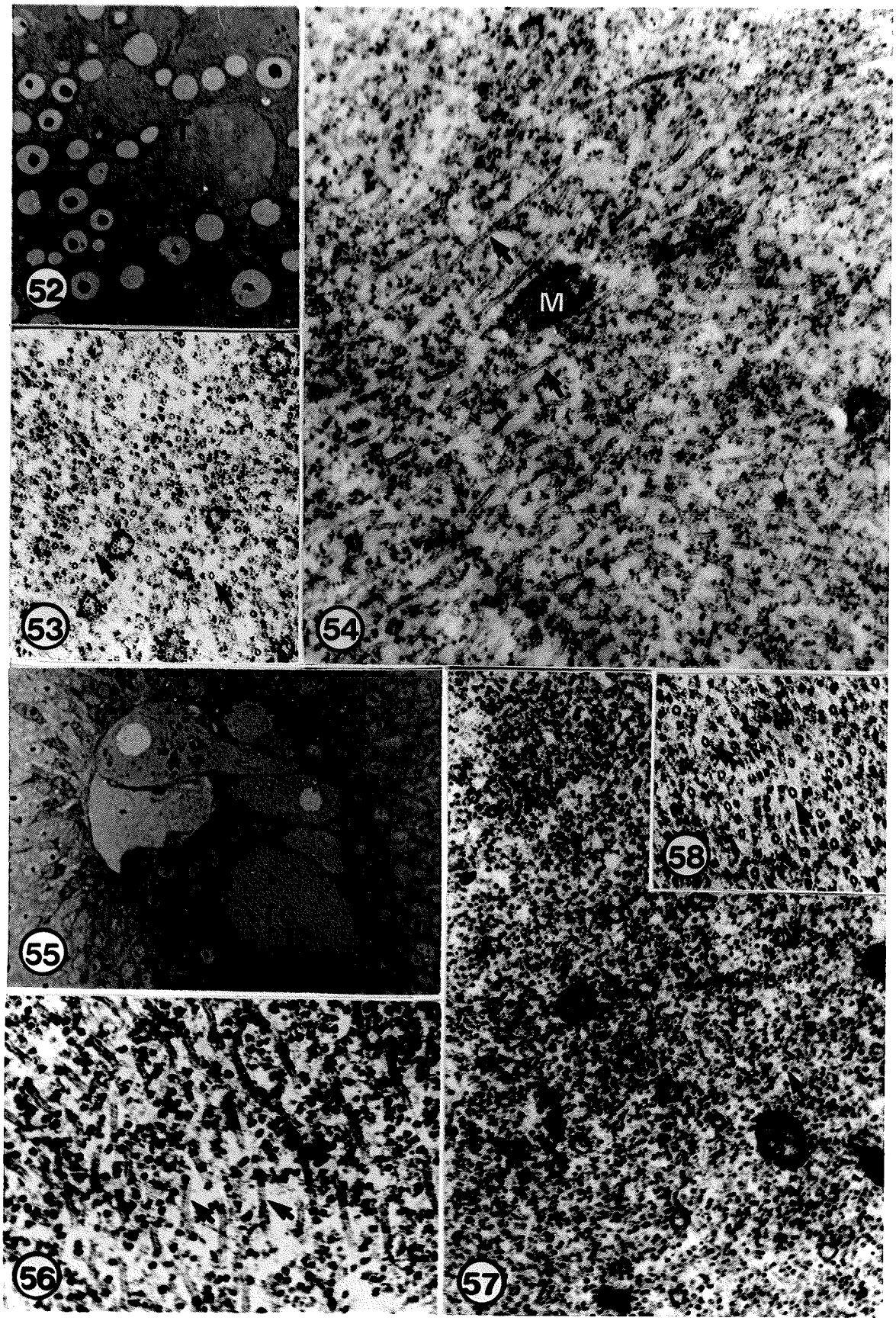
52
53
54
M
55
56
57
58

Plate 12.

1 day post molt.

Figure 59. A polarizing micrograph showing two trophic cords and an early adult core. X150.

Figure 60. This immunofluorescence micrograph, longitudinal section, DGD embedding, shows a large trophic cord and the early adult core. X600.

Figures 61-63. These immunofluorescence micrographs, cross sections, DGD embedding, reveal three large cords (arrows) in the oocyte area (Fig. 61) and both discrete (Fig. 62) and diffuse (Fig. 63) staining in the early adult core. X600, X600, X600.

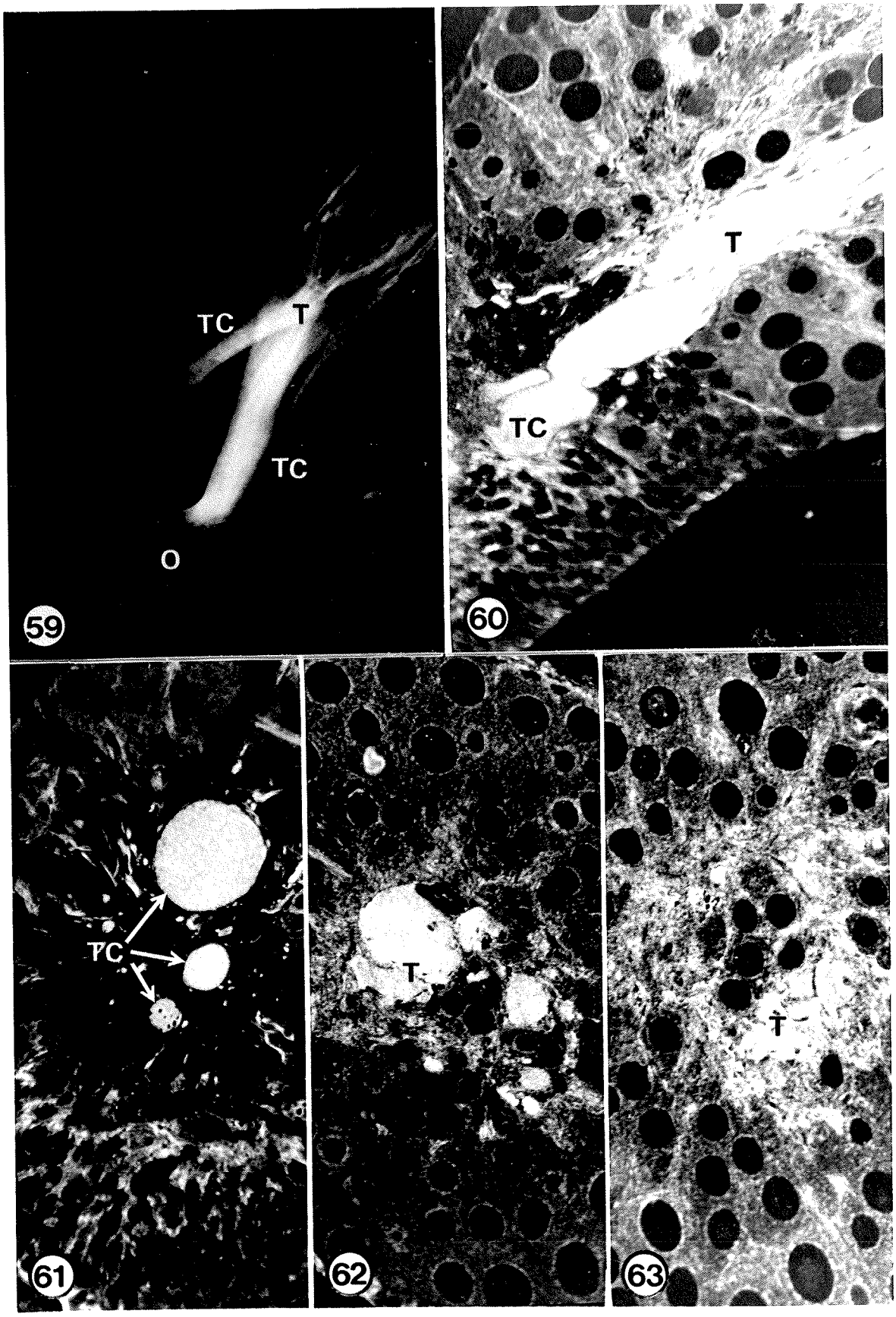
TC
T
TC
O
59
T
TC
60
TC
61
T
62
T
63

Plate 13.

1 day post molt.

Figure 64. A brightfield micrograph, oblique section, showing portion of the oocyte area and the posterior early adult core. X400.

Figures 65-66. These TEMs, cross sections, reveal the longitudinal arrangement of MTs (arrows) in the early adult core. X82,500, X105,000.

Figure 67. This brightfield micrograph, cross section, depicts two large cords. X200.

Figures 68-69. These TEMs, cross sections, show the predominantly longitudinal arrangement of MTs (arrows) in trophic cords. X51,000, X98,000.

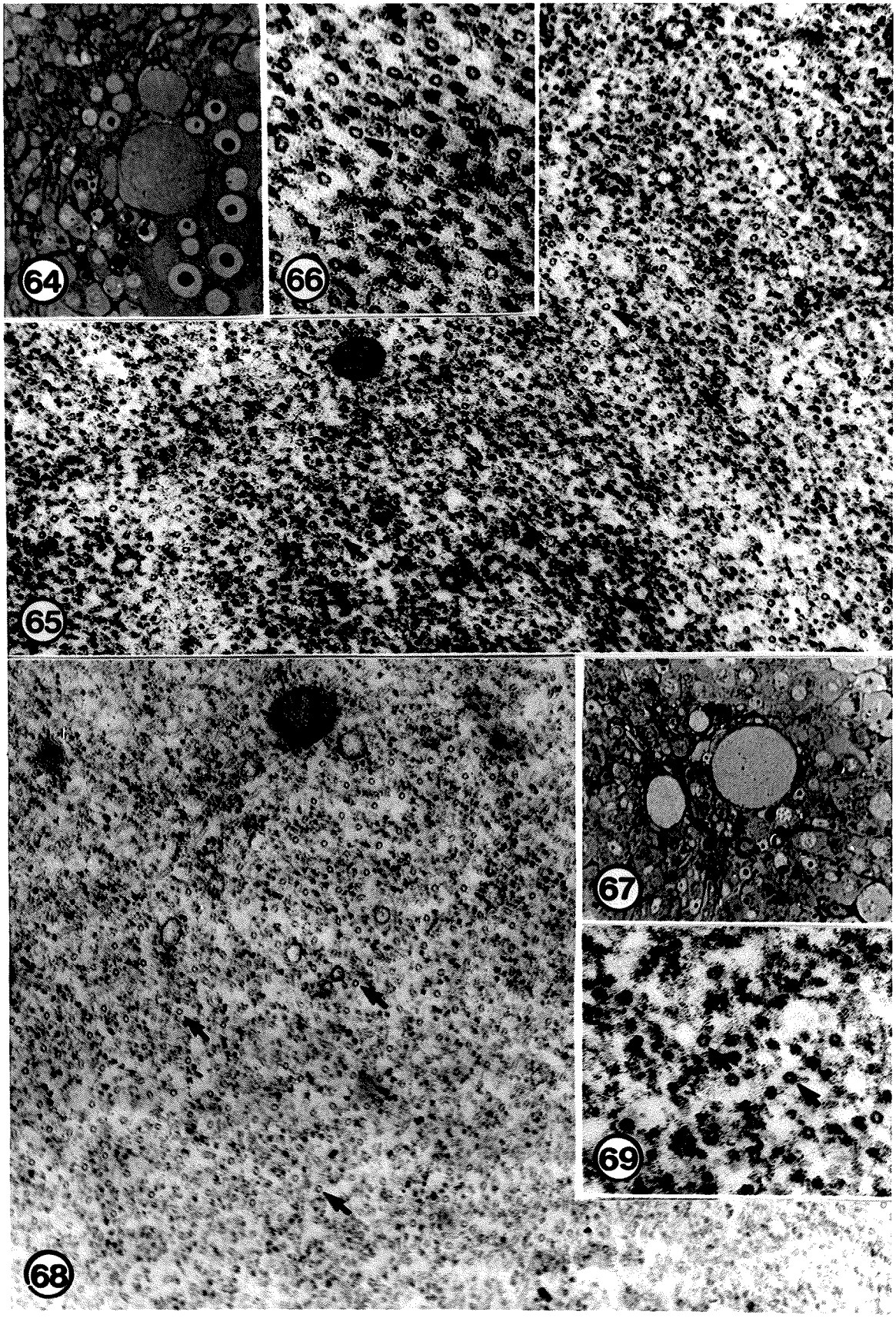
64
66
65
67
69
68

Plate 14.

2 days post molt.

Figure 70. This polarizing micrograph shows trophic cords and the early adult core. X150.

Figures 71-72. Immunofluorescence micrographs, longitudinal sections, DGD embedding, showing large trophic cords and the early adult core. X700, X650.

Figure 73. This immunofluorescence micrograph, oblique sections, DGD embedding, illustrates two large cords in the oocyte area and the posterior early adult core. X400.

Figure 74. An immunofluorescence micrograph of an early adult core, cross section, DGD embedding. X300.

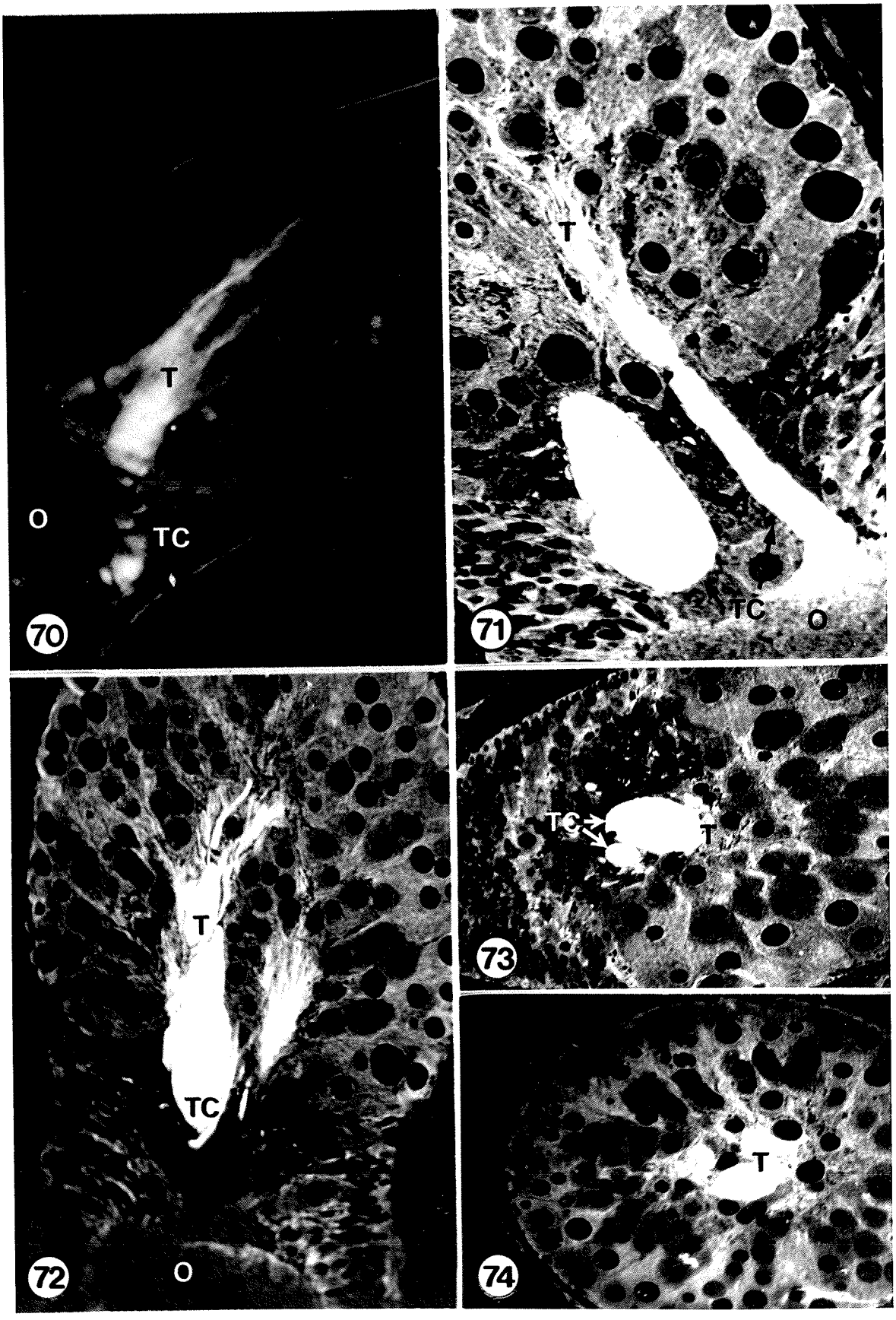
T
O
TC
70
T
TC
O
71
T
TC
72
O
TC
T
73
T
74

Plate 15.

2 days post molt.

Figure 75. A brightfield micrograph showing the early adult core, cross section. X450.

Figures 76-78. These TEMs, cross sections, illustrate the variable appearance of the early adult core. There are membrane-free areas with numerous longitudinally arranged MTs (arrows) (Fig. 76), other membrane-free areas with only scant MTs (arrows) (Fig. 77) and also areas with tortuous membranes (Fig. 78). X46,000, X37,500, X60,500.

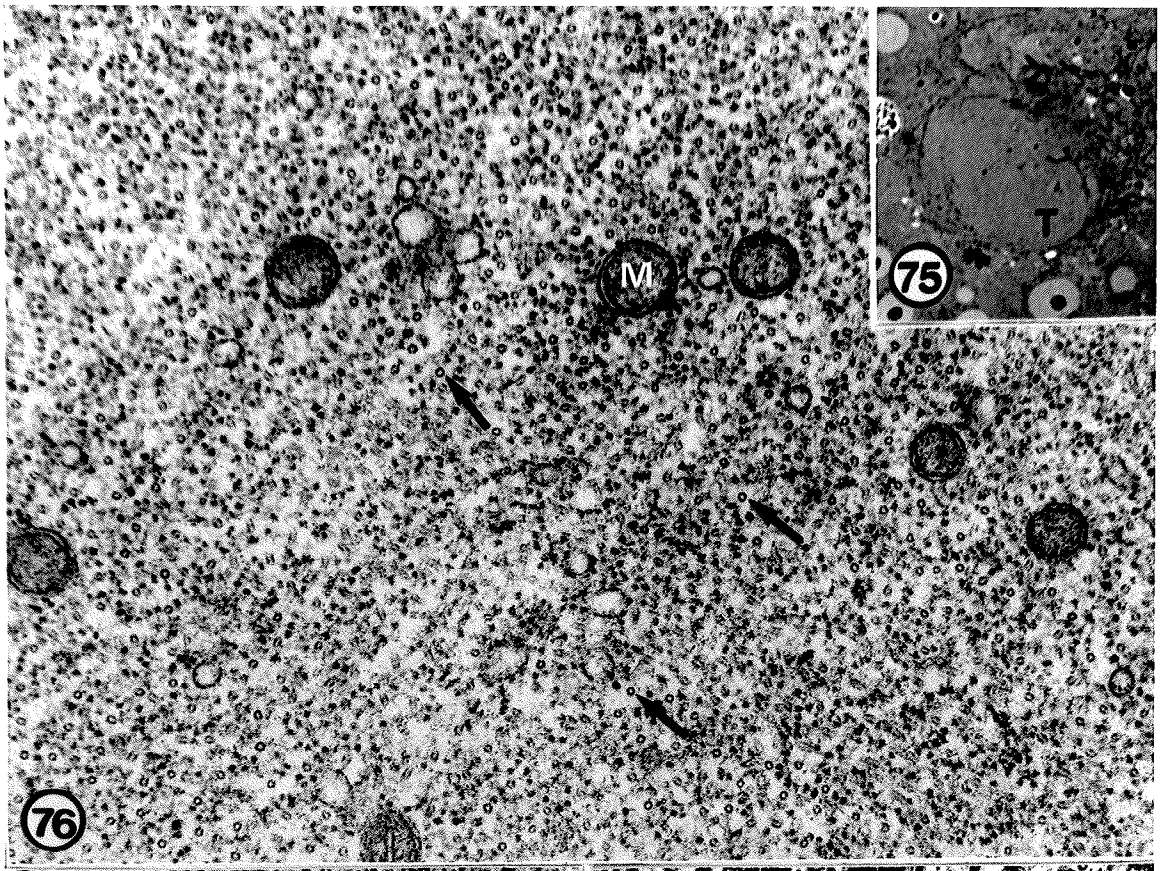
M
T
75
76

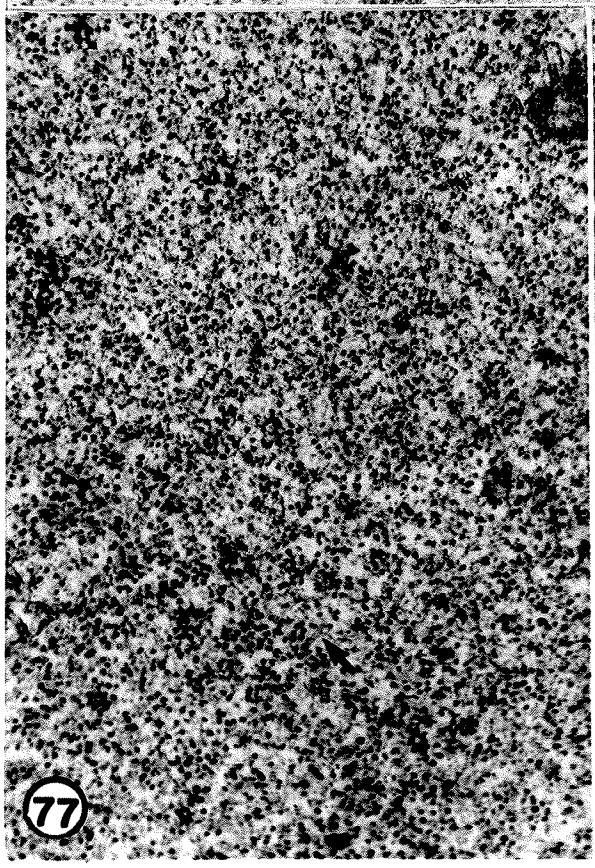
77

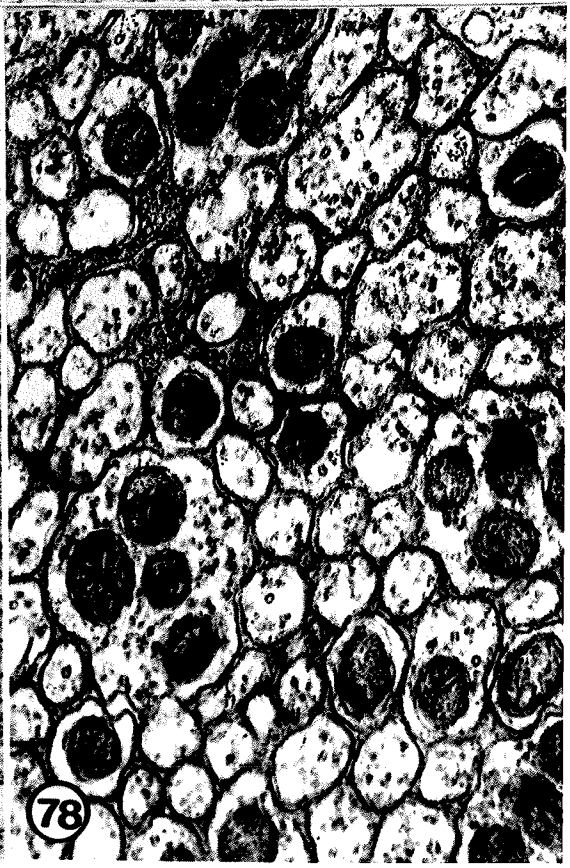
78

Plate 16.

2 days post molt.

Figure 79. This TEM, cross section, shows the high packing density of MTs (arrows) in the large trophic cords. Note that the MTs in this area are perpendicularly arranged. X58,900.

Figure 80. The lower packing density of MTs in small cords is revealed in this TEM, cross section. X35,500.

Figure 81. This TEM, cross section, illustrates the high MT packing density in large cords. X144,000.

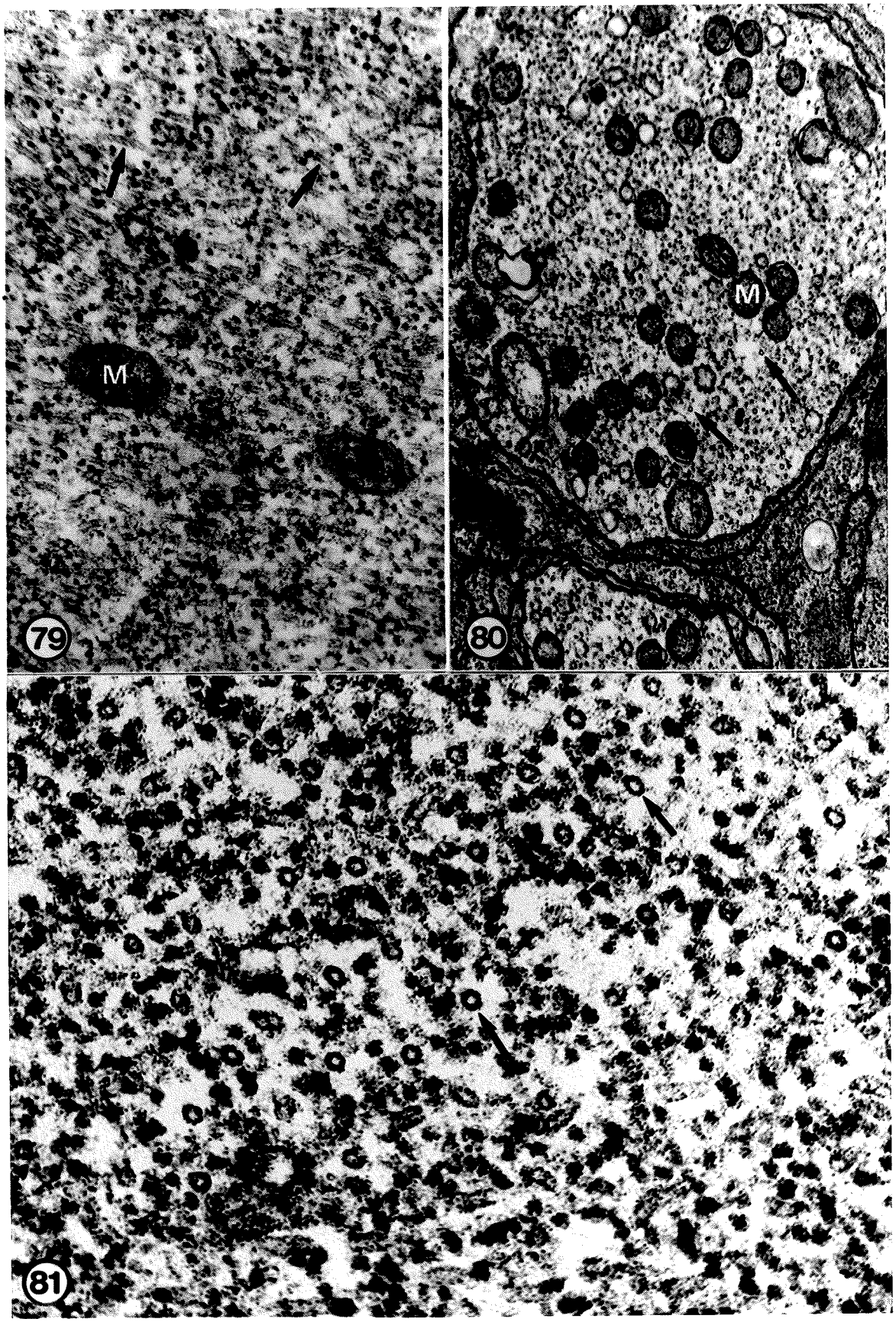
M
79
M
80
81

Plate 17.

Biochemical analysis.

Figure 82. Analysis with the antibody against slime mold β-tubulin. Lanes 1-6 are from an immunostained nitrocellulose membrane and lanes 7 and 8 are from silver stained gels. Lane 1, twice cycled bovine brain tubulin; lane 2, 6 dbm ovariole homogenate; lane 3, 5 dbm ovariole homogenate; lane 4, 4 dbm ovariole homogenate; lane 5, 3 dbm ovariole homogenate; lane 6, 1 dbm ovariole homogenate; lane 7, twice cycled bovine brain tubulin; lane 7, MW markers. The scale on the right hand side represents MW X 10^3

Figure 83. Analysis with the antibody against Tetrahymena tubulin. Lane identification is as in Fig. 82.

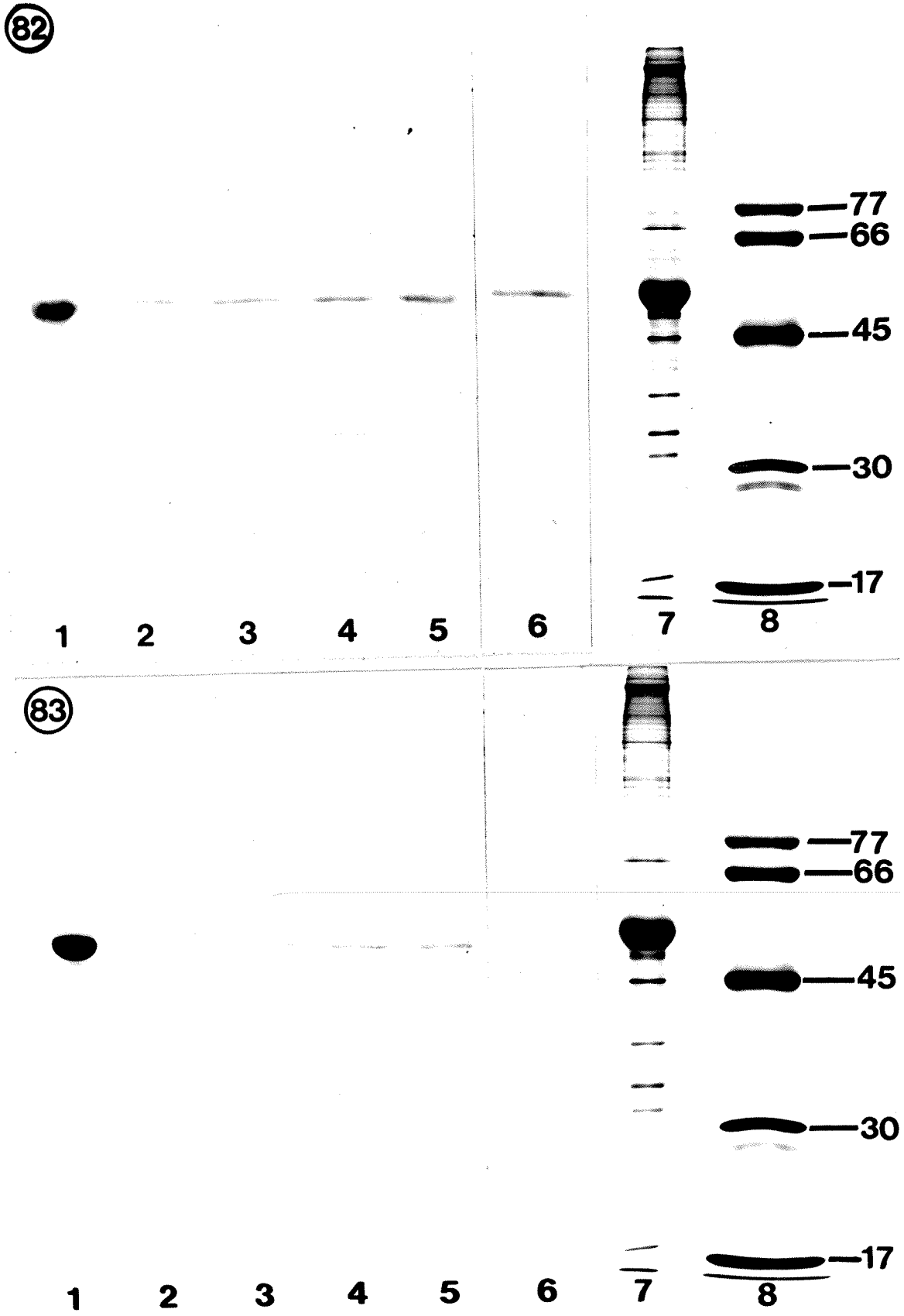
82
77
66
45
30
17
1
2
3
4
5
6
7
8
83
77
66
45
30
17
1
2
3
4
5
6
7
8

Plate 18.

Biochemical analysis.

Figure 84. Silver stained gel after electrophoretic transfer. Note that only high MW proteins remain in the gel.

Figure 85. Control nitrocellulose membrane. This membrane was stained only with the secondary antibody. Note the absence of bands.

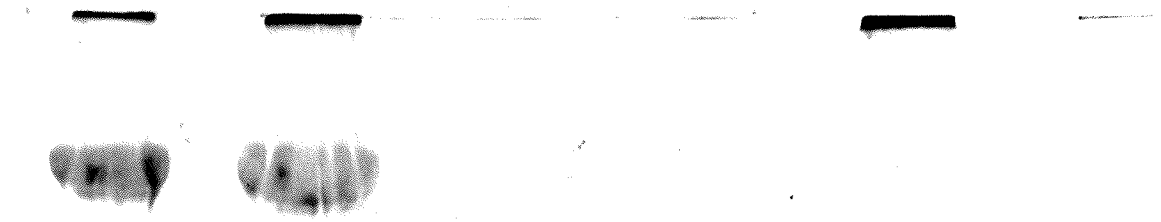

DISCUSSION

The integrated use of TEM, polarizing and immunofluorescence microscopy made it possible to accurately determine the spatial and temporal pattern of MT deployment in the trophic cords and presumptive core. None of these microscopic techniques alone could have yielded this information. MTs are readily identified in TEM and their orientation, arrangement, and density within relatively small areas can be determined. The light microscope offers an advantage over TEM when an overall view of the MT distribution in a tissue is desired, especially if the tissue is large such as the Rhodnius ovariole. Birefringence in the adult trophic core and cords has been shown to be a consequence of a massive MT system (Huebner, 1981). Polarizing microscopy is not, however, specific for MTs, any anisotropic structure will show birefringence in polarized light (Culling, 1974). Immunofluorescence microscopy of sectioned ovarioles offered increased resolution compared to polarizing microscopy of whole ovarioles. Additionally, staining with anti-tubulin antibodies allowed for the specific detection of all tubulin, both monomeric and polymeric. The results from these three microscopic methods therefore complement each other well and in conjunction with the biochemical evidence

lead to the biological conclusions presented below. Since the TEM and polarizing microscopy methods used were routine they will not be discussed further. Immunofluorescence microscopy on tissue sections is still a novel technique, and its use in the present study required numerous adaptations. Aspects of this methodology will therefore be discussed in some detail below.

Immunofluorescence methods

1. Fixations

The criteria used for choosing a fixative for immunofluorescence microscopy include, as is generally true in all microscopy of intact tissues, good overall morphological preservation. In addition, immunofluorescence microscopy places special restraints on the choice of fixative. It has to preserve the specific structure under study and its antigenicity, with minimal background fluorescence being imparted to the tissue.

The fixative buffer used in this study, PHEM buffer 1.0mM GTP (Watson and Huebner, 1986), is based on buffers which maximize recovery of MTs under *in vitro* assembly conditions (Weisenberg, 1972). This buffer was chosen because it stabilizes the MTs during the fixation process (Watson, 1984).

Despite the fact that it was known from early TEM studies that glutaraldehyde is required for the ultrastructural preservation of MTs (Ledbetter and Porter,

1963), it has generally been avoided as a fixative for immunofluorescence microscopy. This is because glutaraldehyde leaves the tissue with a high concentration of free aldehyde groups which bind both primary and secondary antibodies non-specifically, thus imparting high non-specific background to the tissue (Cande et al., 1977; Weber et al., 1978). The non-specific fluorescence can be circumvented by using low glutaraldehyde concentrations and the inclusion of a $NaBH_4$ treatment step which reduces the free aldehyde groups (Weber et al., 1978). The fixative used in this study fulfilled all four criteria outlined above, if $NaBH_4$ treatment was included.

2. Controls

The use of new antibodies in immunological work requires extensive antibody characterization and specificity testing. The antibodies used in this study were either purchased or received as gifts, and had been used in numerous studies previously. The characterization of the specificity of these antibodies was therefore already established. Since mitotic spindles and the MT-rich adult core stained with all four antibodies it gave added confidence in the tubulin specificity of these antibodies.

Autofluorescence can arise from two sources, the inherent fluorescence some tissues possess and from the preparative methods. Autofluorescence can be assessed by bringing the tissue through the staining procedure but

omitting both antibodies. The results show that autofluorescence was very low and not a problem in the present study.

Another type of background fluorescence sometimes arises due to non-specific binding of secondary antibodies to the tissue. This type of background is minimized by blocking such non-specific protein-protein binding with a PBS-BSA step and by diluting the antibodies with a PBS-BSA solution. An assessment of this type of background is best done by bringing the tissue through the staining procedure but omitting the primary antibody. The results from the current study indicate that even though this kind of background was considerable in some cases (see DGD section), it was completely non-specific and did therefore not affect the specific pattern visualized with the anti-tubulin antibodies.

3. Comparison of antibodies

Polyclonal anti-tubulin antibodies generally show a high degree of species cross-reactivity (Weber and Osborn, 1979). This is not unexpected since tubulin is a highly conserved protein evolutionarily (Cleveland and Sullivan, 1985). Most monoclonal anti-tubulin antibodies also recognize common epitopes and therefore bind to tubulins from a variety of animal species. There are, however, monoclonal anti-tubulin antibodies available which recognize unique epitopes present only on certain species, tissue, or

cell specific tubulin isotypes (Birkett et al., 1985; Cleveland and Sullivan, 1985). All four primary antibodies used in the present study had been shown previously to react to tubulin from a broad range of animals (Fujiwara and Pollard, 1978; Watson, personal communication). As mentioned before all four antibodies stained mitotic spindles and adult trophic cores, and no difference was observed in the staining pattern these antibodies produced. These facts and the well characterized nature of these antibodies make it possible to be confident that the results accurately reflect the in situ tubulin distribution.

4. The use of PEG as an embedding medium

As mentioned in the introduction the methods for indirect immunofluorescence localization of cytoskeletal proteins have primarily been used on very thinly spread cells, grown in culture. Numerous methods have been devised to localize cytoskeletal elements in tissue sections (see introduction). None of these, with the exception of PEG, appeared to be satisfactory for high resolution immunofluorescent localization of MTs.

Recent use of PEG was initiated with its utilization as an extractable embedding medium for TEM (Wolosewick, 1980). Subsequently a few studies have adapted it for use in immunofluorescence microscopy of intact tissues (Repetto-Antoine et al., 1982; Wolosewick and De Mey, 1982; Parysek et al., 1984). The major challenge the use of PEG posed in

this study was in overcoming the difficulty encountered in obtaining flat sections. Because PEG sectioning was performed on dry knives, some compression of the tissue and curling up of the sections was unavoidable. When these sections are tacked down on a dry coverslip and heated they frequently form folds. The most likely reason for this is if there are two points in the section where it is firmly stuck to the coverslip and there is a bulge in the section between these attachment points. When the section warms up the PEG melts and the bulge in the tissue sinks to the surface of the coverslip. Because the attachment points are firm and not free to move the extra length of tissue forms creases and folds. This problem was partially overcome by floating the sections on a liquid. The section can then flatten out before any contact is made with the coverslip surface. Water was initially used as a flattening liquid but its use was discontinued when it was discovered that 50.0% glycerol gave much more consistent, even staining. The uneven staining attained with water was assumed to be due to the loss or masking of tubulin antigenic sites caused by air exposure. Wolosewick (1980) reported that PEG sections flattened on water showed extensive air drying damage in the TEM. Apparently the high surface tension of water prevents it from moving rapidly enough by capillary action through the section to cover exposed surface as the PEG dissolves. Lower surface tension liquids such as 50.0% glycerol moves much faster through the tissue, covering

surfaces as they become exposed. The possibility of air exposure damage was further minimized by covering the sections with pure glycerol.

In previous studies employing PEG, the blocks have been hardened by cooling them rapidly in liquid nitrogen (Wolosewick, 1980; Repetto-Antoine et al., 1982; Wolosewick and De Mey, 1982; Parysek et al., 1984). In order to simplify procedures the possibility of cooling the blocks slowly at room temperature was evaluated in the present study. Since no adverse effects were observed on the tissue with this modification, it was adopted for use in all subsequent experiments.

In general PEG appears to be well suited as an embedding medium in studies such as the one reported here. The one major drawback of PEG embedding is the difficulty in obtaining flat sections. This situation, however, can be improved considerably by implementing the appropriate adaptations as described.

5. The use of DGD as an embedding medium

The use of DGD in the present study was spurred on by recent reports on the use of this medium for TEM (Capco et al., 1984; Capco and McGaughey, 1986). Since DGD is water insoluble, DGD embedded tissue could be sectioned directly onto water, thereby allowing the sections to flatten and greatly reducing the incidence of folds. In addition to TEM, DGD has been used previously as an embedding medium for

routine histology (Salazar, 1964), for the direct immunofluorescence localization of insulin in the pancreas (Lacy and Davies, 1959), and for the indirect immunofluorescence localization of crystallins in the frog lens (Taleporos, 1974).

Based on my study DGD is deemed highly suitable as an embedding medium for immunofluorescent localization of tubulin in intact tissues. The successful application of DGD to the indirect immunofluorescence localization of tubulin in the present study suggests that DGD may be generally applicable for such localizations of cytoskeletal proteins.

6. Comparison of PEG and DGD

PEG and DGD both proved to be applicable for the purpose of this study. Both media have the potential to give high resolution immunofluorescent images of very good quality. Each has its pros and cons though (see Table 1). It is felt, however that DGD is preferable for studies such as this one since quality sections can be obtained more easily than with PEG.

A feature of both these media, which was not exploited in the present study, is that they can be sectioned for TEM. Immunofluorescence and TEM images could therefore be obtained from the same block, even the same cell.

This is the first report on the use of indirect immunofluorescence localization of cytoskeletal proteins in

PEG embedded material from non-mammalian sources and in DGD embedded material from any source. With the choice now of two embedding media for the immunofluorescent localization of cytoskeletal proteins in intact tissues, at least one of these should prove to be suitable for most applications.

The development of MTs in the trophic core and cords

The biological objective of this study was to link the changes in tubulin levels and the appearance of MTs in the trophic core and cords to each other and to a developmental timeframe. Previous studies on the post-embryonic development of Rhodnius prolixus have used the time of feeding as a temporal reference point (Buxton, 1930; Case, 1970; Lutz and Huebner, 1980, 1981). A case can be made for using the time feeding as a temporal reference point since it is feeding which sets in motion the series of physiological changes that will ultimately culminate in molting. However, survey of these previous studies indicates variability. Buxton (1930) reports that at 24°C animals molt at 22 dpf and at 30°C they molt at 15 dpf, Case (1970) reports that at 28°C two separate colonies molt at 19 dpf and 22 dpf, in Lutz and Huebner's (1980, 1981) studies the animals molted 21 dpf at 27°C. In the present study, at 26°C, considerable variability in molting time was observed, with an average molting time of 26 dpf. The slower development observed under the rearing conditions in this study is surprising since Buxton (1930) found development to

be faster at 24°C than the present study did at 26°C. Humidity is also known to affect developmental rates but all of the studies above used high humidity so this factor is unlikely the source of the variability. Finally, the amount of blood ingested might be thought to influence the time required to molt. This does not explain, however, the results from this study for two reasons. One is that a high variability is unlikely to arise from such a narrow weight range of ingested blood as used in the present study. Secondly, Friend et al. (1965) found that as long as instars ingested the minimum amount of blood required to molt they molted at the same time, i. e. any blood beyond the minimal amount required did not speed up development. The cause for the change in time from feeding to molt in the fifth instar Rhodnius found in this study is enigmatic and warrants further study.

The decision to use the larval-adult molt as the temporal reference point was made in an attempt to mitigate some of the problems with using time of feeding as a reference point. One thus assumes that the ovaries from two animals which had just molted were at a similar developmental stage, even though the number of days between feeding and molting differed considerably between the two animals. This timing strategy is quite accurate for ovarioles examined post-molt, because it is known when the individuals molted. The staging of ovarioles to be examined pre-molt is somewhat less accurate however. The reason for

this is that it is based on the average molting day for that group and the particular individual under study may have been developing at a rate which was either faster or slower than the average. This may explain some of the variability observed in pre-molt ovarioles.

From the present study the developmental sequence of events involved in the appearance of MTs in the trophic core and cords during the larval-adult transformation of Rhodnius prolixus can be summarized as follows. Prior to 6 dbm the presumptive core is largely devoid of MTs and there are no MT containing cords. This statement is based on polarizing microscopy which does not identify the small cords connected to oocytes which have not yet initiated pre-vitellogenic growth. It is quite conceivable that immunofluorescence microscopy would have demonstrated MTs in these cords. The first oocyte initiates pre-vitellogenic growth by 6 dbm and the cord connecting this oocyte to the presumptive core appears to contain a full complement of MTs one or two days later. As this oocyte grows and moves posteriorly the cord lengthens and widens apparently with the concomitant build-up of MTs within it. This cord widening and MT build-up is uniform along the entire length of the cord, i. e. it is not initiated at one end and then passed along the length of the cord.

First appearance of an MT system within the larval-core is also about 6 dbm. This MT appearance is very distinct in that it is non-uniform, i. e. the MTs which appear are not

distributed uniformly throughout the nucleus-free, core-like area. Rather they seem to be localized only in certain cord-like areas within the presumptive core. Some of the areas devoid of MTs are occupied by very elaborate membrane systems whereas others are mainly occupied by ribosomes. This situation is observed throughout the time period investigated in the present study, but as development proceeds there is an increase in the number and size of MT containing areas. In most post-molt ovarioles some of these areas fuse together or individual ones flare out, thus forming the earliest stages of the adult core.

The first sign that a second oocyte has initiated pre-vitellogenic growth is seen 3 dbm and the third one initiates pre-vitellogenic growth either 0 dpm or 1 dpm. The trophic cords connected to these oocytes undergo the same changes as the first cord, i. e. they become packed with MTs as they grow in length and width.

The orientation of the MTs in the cords and presumptive trophic core through the period of appearance is predominantly longitudinal. Occasionally though MTs are arrange this feature being much more frequent in the presumtive core than cords.

The picture which emerges from this study is that small MT containing cords enlarge as the oocytes to which they are connected begin pre-vitellogenic growth. As these cords enlarge the MTs are continually added such that there is no apparent difference in MT density between the cord connected

to the first pre-vitellogenic oocyte and the second or third. No difference in MT density was observed along the length of the trophic cords either. These findings are in close agreement with a previous report on the formation of trophic cords in Dysdercus (Hyams and Stebbings, 1979b). The MT density in the small cords connected to quiescent oocytes is somewhat lower than in cords connected to growing oocytes. The situation in the core area is much more complex which makes it difficult to decipher the mechanism which leads to formation of the MT packed adult-core. Perhaps the best explanation for the observed facts can be arrived at by considering the model for the origin of the nurse cell-oocyte syncytium proposed by Huebner and Anderson (1972c). In this model the adult syncytium arises from the fusion of a number of separate sibling syncytial clusters. The larval-core is a complex entanglement of cell processes including the small cords connecting the quiescent oocytes and their respective sibling clusters. These small cords contain some MTs but as they grow concurrently with their oocytes they become packed with MTs. It is quite

conceivable then that the MT containing cord-like structures seen in the presumtive core are actually the anterior portions of trophic cords. These will subsequently fuse during the restructuring of the core area thus forming the MT packed adult trophic core. What began as a MT rich cord between an oocyte and its sibling nurse cell cluster is thus

transformed, through membrane fusions, into a portion of the MT packed trophic core common to all the sibling clusters in the ovariole.

It is interesting to note that a mature adult-core, such as seen in vitellogenic adult ovarioles, was not observed within the time frame of this study (i. e. before 2 dpm). An early adult-core was in place by 1 dbm or 0 dpm but it may be that a blood meal is required by the adult imago for the formation of the mature adult-core.

The core MT density, as determined in the present study, showed a gradual increase from 2 dbm to 2 dpm. It should be emphasized however that these results are based on preliminary data only. Both small sample size and difficulty encountered in positively identifying core areas and cords for counting, make this finding only suggestive. These results indicate further examination of both cords and core area MT packing should be done.

The level of tubulin as a proportion of total ovariole protein appears to increase from 6 dbm to at least 3 dbm. The two antibodies gave different results for the relative level of tubulin at 1 dbm. Whether there is an increase or a decrease in the tubulin level on 1dbm cannot be determined from the data collected in this study. One might, however, expect that the level would increase since all the microscopic observations indicate an increase in the size of the MT arrays. The biochemical results indicate a concomitant increase in tubulin levels with the increase in

length and number of assembled MTs during the same period. These findings are consistent with the hypothesis that MT assembly from a tubulin pool coincides with new synthesis of tubulin so that the concentration of unpolymerized tubulin is mainained constant. The alternative hypothesis, namely that a large pre-existing pool of tubulin is present by the onset of MT assembly (i. e. about 6 dbm) and that MTs are then assembled from this pre-existing pool without new tubulin synthesis , is not supported by my results. This agrees with the evidence from tissue culture cells (Kirschner and Mitchison, 1986).

In conclusion, this study has confirmed the usefulness of PEG as an embedding medium for immunofluorescence microscopy of whole tissue and in addition has extended the use of this material to include invertebrate tissue. DGD was shown, for the first time, to be applicable as an embedding medium for immunofluorescence microscopy of cytoskeletal proteins. DGD was found to be preferable to PEG for the purpose of this study.

Biologically, the first appearance of MTs was in trophic cords at 6 dbm. MTs grow in length and numbers as the cords grow. The MT packed adult-core arises from the fusion of the anterior portions of MT containing trophic cords. A mature adult-core did not fully form by 2 dpm. This study provides a framework for further investigations into the mechanisms and patterns of tubulin synthesis and MT assembly in this remarkably complex yet very interesting model cell system.

LITERATURE CITED

Amos, L. A., R. W. Linck, and A. Klug. 1976. Molecular structure of flagellar microtubules. IN Cell motility. Book C. Microtubules and related proteins. R. Goldman, T. Pollard, & J. Rosenbaum (eds.). Cold Spring Harbour Laboratory, Cold Spring Harbor. pp. 847-867.

Anderson, E., and H. W. Beams. 1956. Evidence from electron micrographs for the passage of material through pores of the nuclear membrane. J. Biophys. and Biochem. Cytol. 2(4): 439-443.

Anderson, W. A., and R. A. Ellis. 1965. Ultrastructure of Trypanosoma lewisi flagellum, microtubules and the kinetoplast. J. Protozool. 12: 484-499.

Bennett, C. E., and H. Stebbings. 1979. Redundant nutritive tubes in insect ovarioles: the fate of an extensive microtubule transport system. Cell Biol. Int. Rep. 3(7): 577-583.

Bergen, L. G., and G. G. Borisy. 1980. Head-to-tail polymerization of microtubules in vitro. J. Cell Biol. 84(1): 141-150.

Birkett, C. R., K. E. Foster, L. Johnson, and K. Gull. 1985. Use of monoclonal antibodies to analyse the expression of a multi-tubulin family. FEBS lett. 187(2): 211-218.

Bonhag, P. F. 1955. Histochemical studies of the ovarian nurse tissues and oocytes of the milkweed bug, Oncopeltus fasciatus (Dallas). 1. J. Morph. 96(3): 381 -440.

Bonhag, P. F. 1958. Ovarian structure and vitellogenesis in insects. Ann. Rev. Enotomol. 3: 137-160.

Borisy, G. G., J. M. Marcum, J. B. Olmsted, D. B. Murphy, and K. A. Johnson. 1975. Purification of tubulin and associated high molecular weight proteins from porcine brain and characterization of microtubule assembly in vitro. Ann. N. Y. Acad. Sci. 253: 107-132.

Brunt, A. M. 1970. Extensive system of microtubules in the ovariole of Dysdercus fasciatus Signoret (Heteroptera, Pyrrhocoridae). Nature 228: 80-81.

Büning, J. 1972. Untersuchungen am Ovar von Bruchidius obtectus Say. (Coleoptera-Polyphaga) zur Klärung des Oocytenwachstums in der Prävitellogenese. Z. Zellforsch. 128: 241-282.

Büning, J. 1979a. The trophic tissue of telotrophic ovarioles in polyphage Coleoptera. Zoomorph. 93: 33- 50.

Büning, J. 1979b. The telotrophic nature of ovarioles of polyphage Coleoptera. Zoomorh. 93: 51-57.

Büning, J. 1980. The ovary of Raphidia flavipes is telotrophic and of the Sialis type (Insecta, Raphidoptera). Zoomorph. 95: 127-131.

Bussolati, G., V. Alfani, K. Weber, and M. Osborn. 1980. Immunocytochemical detection of actin on fixed and embedded tissues: its potential use in routine pathology. J. Histochem. Cytochem. 28(2): 169-173.

Buxton, P. A. 1930. The biology of a blood-sucking bug, Rhodnius prolixus. Trans. Ent. Soc. London 78(2): 227-236.

Cande, W. Z., E. Lazarides, and J. R. McIntosh. 1977. A comparison of the distribution of actin and tubulin in the mammalian mitotic spindle as seen by indirect immunofluorescence. J. Cell Biol. 72(3): 552-567.

Capco, D. G., and W. R. Jeffry. 1979. Origin and spatial distribution of maternal messenger RNA during oogenesis of an insect, Oncopeltus fasciatus. J. Cell Sci. 39: 63-76.

Capco, D. G., G. Krochmalnic, and S. Penman. 1984. A new method of preparing embeddment-free sections for transmission electron microscopy: applications to the cytoskeletal framework and other three dimensional networks J. Cell Biol. 98: 1878-1885.

Capco, D. G., and R. W. McGaughey. 1986. Cytoskeletal reorganization during early mammalian development: analysis using embedment-free sections. Dev. Biol. 115: 446-458.

Case, D. 1970. Postembryonic development of the ovary of Rhodnius prolixus Stål. M. Sc. thesis. Department of Zoology, McGill University, Montreal, Quebec, Canada. 113 p.

Choi, W. C., and W. Nagl. 1977. Patterns of DNA and RNA synthesis during the development of ovarian nurse cells in Gerris najas (Heteroptera). Dev. Biol. 61: 262-272.

Cleveland, D., and M. Kirschner. 1982. Autoregulatory control of the expression of α- and β-tubulins: implications for microtubule assembly. Cold Spring Harbor Symp. Quant. Biol. 46: 783-790.

Cleveland, D. W., and K. F. Sullivan. 1985. Molecular biology and genetics of tubulin. Ann. Rev. Biochem. 54: 331-365.

Coudrier, E., H. Reggio, and D. Louvard. 1982. The cytoskeleton of intestinal microvilli contains two polypeptides immunologically related to proteins of striated muscle. Cold Spring Harbor Symp. Quant. Biol. 46: 881-892.

Culling, C. F. A. 1974. Modern microscopy. Elementary theory and practice. Butterworths & Co. (Canada) Ltd. Toronto. 148 p.

Davenport, R. 1974. Synthesis and intercellular transport of ribosomal RNA in the ovary of the milkweed bug Oncopeltus fasciatus. J. Insect Physiol. 20: 1949-1956.

Davenport, R. 1976. Transport of ribosomal RNA into the oocytes of the milkweed bug, Oncopeltus fasciatus. J. Insect Physiol. 22: 925-926.

Davidson, E. H. 1986. Gene activity in early development. Third edition. Academic Press, Inc., Orlando. 670 p.

Dentler, W. L., S. Granett, G. B. Witman, and J. L. Rosenbaum. 1974. Directionality of brain microtubule assembly in vitro. Proc. Natl. Acad. Sci. USA 71(5): 1710-1714.

Drubin, D. G., S. C. Feinstein, E. M. Shooter, and M. W. Kirschner. 1985. Nerve growth factor-induced neurite outgrowth in PC 12 cells involves the coordinate induction of microtubule assembly and assemblypromoting factors. J. Cell Biol. 101(5): 1799-1807.

Duspiva, F., K. Schaller, D. Weiss, and H. Winter. 1973. Ribonucleinsäuresynthese in der telotroph-meroistischen Ovariole von Dysdercus intermedius Dist. (Heteroptera, Pyrrhoc.). Wilhelm Roux's Arch. 172: 83-130.

Dustin, P. 1984. Microtubules. Springer-Verlag, Berlin. 482 p.

Eschenberg, K. M., and H. L. Dunlap. 1966. The histology and histochemistry of oogenesis in the water strider, Gerris remigis Say. J. Morph. 118: 297-316.

Euteneuer, V., and J. R. McIntosh. 1980. Polarity of midbody and phragmoplast microtubules. J. Cell Biol. 87(2): 509-515.

Euteneuer, V., and J. R. McIntosh. 1981a. Structural polarity of kinetochore microtubules in PtK1 cells. J. Cell Biol. 89(2): 338-345.

Euteneuer, V., and J. R. McIntosh. 1981b. Polarity of some motility-related microtubules. Proc. Natl. Acad. Sci. USA 78(1): 372-376.

Franke, W. W., E. Schmid, M. Osborn, and K. Weber. 1978. Different intermediate filaments distinguished by immunofluorescence microscopy. Proc. Natl. Acad. Sci. USA 75(10): 5034-5038.

Friend, W. G., C. T. H. Choy, and E. Cartwright. 1965. The effect of nutrient intake on the development and the egg production of Rhodnius prolixus Stål (Hemiptera: Reduviidae). Can. J. Zool. 43(6): 891-904.

Fujiwara, K., and T. D. Pollard. 1978. Simultaneous localization of myosin and tubulin in human tissue culture cells by double antibody staining. J. Cell Biol. 77(1): 182-195.

Geuze, H. J., J. W. Slot, P. A. Van Der Ley, and R. C. T. Scheffer. 1981. Use of colloidal gold particles in double-labeling immunoelectron microscopy of ultrathin frozen tissue sections. J. Cell Biol. 89(3): 653-665.

Gorbsky, G. J., P. J. Sammak, and G. G. Borisy. 1987. Chromosomes move poleward in anaphase along stationary microtubules that coordinately disassemble from their kinetochore ends. J. Cell Biol. 104(1): 9-18.

Haimo, L. T. 1982. Dynein decoration of microtubules - determination of polarity. In Methods in cell biology. Volume 24. The cytoskeleton . Part A. L. Wilson (ed.). Academic Press, New York. pp. 189-206.

Haimo, L. T., B. R. Telzer, and J. L. Rosenbaum. 1979. Dynein binds to and crossbridges cytoplasmic microtubules. Proc. Natl. Acad. Sci. USA 76(11): 5759-5763.

Hamon, C., and R. Folliot. 1969. Ultrastructure des cordons trophiques de l`ovaire de divers Homopteres Auchenorhynches. C. R. Acad. Sci. (Paris) D 268: 577-580.

Hogan, D. L., and G. H. Smith. 1982. Unconventional application of standard light and electron immunocytochemical analysis to aldehyde-fixed, araldite-embedded tissues. J. Histochem. Cytochem. 30(12): 1301-1306.

Huebner, E. 1981. Nurse cell-oocyte interaction in the telotrophic ovarioles of an insect, Rhodnius prolixus. Tissue Cell 13(1): 105-125.

Huebner, E. 1982. Ultrastructure and development of the telotrophic ovary. In The ultrastructure and functioning of insect cells. H. Akai, R. C. King, & S. Morohoshi, (eds.). The Society for Insect Cells. Japan. pp. 9-12.

Huebner, E. 1984a. The ultrastructure and development of the telotrophic ovary. In Insect ultrastructure. Volume 2. R. C. King & H. Akai, (eds.). Plenum Press, New York. pp. 3-48.

Huebner, E. 1984b. Developmental cell interactions in female insect reproductive organs. In Advances in invertebrate reproduction. Volume 3. W. Engels (ed.). Elsevier Science Publishers B. V., Amsterdam. pp. 97-105.

Huebner, E., and E. Anderson. 1970. The effects of vinblastine sulfate on the microtubular organization of the ovary of Rhodnius prolixus. J. Cell Biol. 46: 191-198.

Huebner, E., and E. Anderson. 1972a. A Cytological study of the ovary of Rhodnius prolixus. 1. The ontogeny of the follicular epithelium. J. Morph. 136(4): 459-494.

Huebner, E., and E. Anderson. 1972b. A cytological study of the ovary of Rhodnius prolixus. 11. Oocyte differentiation. J. Morph 137(4): 385-415.

Huebner, E., and E. Anderson. 1972c. A cytological study of the ovary of Rhodnius prolixus. 111. Cytoarchitecture and development of the trophic chamber. J. Morph. 138: 1-40.

Hyams, J. S., and H. Stebbings. 1977. The distribution and function of microtubules in nutritive tubes. Tissue Cell 9(3): 537-545.

Hyams, J. S., and H. Stebbings. 1979a. The mechanism of microtubule associated cytoplamic transport. Cell Tissue Res. 196: 103-116.

Hyams, J. S., and H. Stebbings. 1979b. The formation and breakdown of nutritive tubes-massive microtubular organelles associated with cytoplasmic transport. J. Ultrastrct. Res. 68: 46-57.

Indi, S., G. Wakley, and H. Stebbings. 1985. Does freeze-substitution reveal the hydrophobic nature of interprotofilament bonding in microtubules ? Cell Biol. Int. Rep. 9(9): 859-865.

Inoué, S., and K. Dan. 1951. Birefringence of the dividing cell. J. Morph. 89(3): 423-455.

King, R. C., and J. Büning. 1985. The origin and functioning of insect oocytes and nurse cells. In Comprehensive insect physiology, biochemistry and pharmacology. Volume 1. G. A. Kerkut & L. I. Gilbert (eds.). Pergamon Press, Toronto. pp. 37-82.

Kirschner, M., and T. Mitchison. 1986. Beyond self-assembly: from microtubules to morphogenesis. Cell 45: 329-342.

Kramer, J. M. 1981. Immunofluorescent localization of PGK-1 and PGK-2 isozymes within specific cells of the mouse testis. Dev. Biol. 87: 30-36.

Lacy, P. E., and J. Davies. 1959. Demonstration of insulin in mammalian pancreas by the fluorescent antibody method. Stain Techn. 34: 85-89.

Laemmli, U. K. 1970. Cleavage of structural proteins during the assembly of the head of bacteriophage T_4. Nature 227: 680-685.

Ledbetter, M. C., and K. R. Porter. 1963. A "microtubule" in plant cell fine structure. J. Cell Biol. 19: 239-250.

Lowry, O. N., N. J. Rosebrough, A. L. Farr, and R. J. Randall. 1951. Protein measurement with the Folin phenol reagent. J. Biol. Chem. 193: 265-275.

Luftig, R. B., P. N. McMillan, J. A. Weatherbee, and R. R. Weihing. 1977. Increased visualization of microtubules by an improved fixation procedure. J. Histochem. Cytochem. 25(3): 175-187.

Lutz, D. A., and E. Huebner. 1980. Development and cellular differentiation of an insect telotrophic ovary (Rhodnius prolixus). Tissue Cell 12(4): 773-794.

Lutz, D. A., and E. Huebner. 1981. Development of nurse cell-oocyte interactions in the insect telotrophic ovary (Rhodnius prolixus). Tissue Cell 13(2): 321-335.

MacGregor, H. C., and H. Stebbings. 1970. A massive system of microtubules associated with cytoplasmic movement in telotrophic ovarioles. J. Cell Sci. 6: 431-449.

Maddrell, S. H. P. 1969. Secretion by the Malpighian tubules of Rhodnius. The movements of ions and water. J. Exp. Biol. 51: 71-97.

Matus, A., R. Bernhardt, and T. Hugh-Jones. 1981. High molecular weight microtubule-associated proteins are preferentially associated with dendritic microtubules in brain. Proc. Natl. Acad. Sci. USA 78(5): 3010-3014.

Maupin, P., and T. D. Pollard. 1983. Improved preservation and staining of HeLa cell actin filaments, clathrin coated membranes and other cytoplasmic structures by tannic acid-glutaraldehyde-saponin fixation. J. Cell Biol. 96(1): 51-62.

Mays, U. 1972. Stofftransport im Ovar von Pyrrhocoris apterus L. Z. Zellforsch. 123: 395-410.

McIntosh, J. R., and V. Euteneuer. 1984. Tubulin hooks as probes for microtubule polarity: an analysis of the method and an evaluation of data on microtubule polarity in the mitotic spindle. J. Cell Biol. 98(2): 525-533.

McKeithan, T. W., and J. L. Rosenbaum. 1984. The biochemistry of microtubules. A review. In Cell and muscle motility. Volume 5. The cytoskeleton. J. W. Shay (ed.). Plenum Press, New York. pp. 255-288.

Miller, R. H., and R. J. Lasek. 1985. Cross-bridges mediate anterograde and retrograde vesicle transport along microtubules in squid axoplasm. J. Cell Biol. 101(6): 2181-2193.

Mitchison, T., L. Evans, E. Schulze, and M. Kirschner. 1986. Sites of microtubule assembly and disassembly in the mitotic spindle. Cell 45 : 515-527.

Murphy, D. B., W. A. Grasser, and K. T. Wallis. 1986. Immunofluorescence examination of beta tubulin expression and marginal band formation in developing chicken erythroblasts. J. Cell Biol. 102(2): 628-635.

Osborn, M., and K. Weber. 1982. Immunofluorescence and immunocytochemical procedures with affinity purified antibodies: tubulin containing structures. In Methods in cell biology. Volume 24. The cytoskeleton. Part A. L. Wilson (ed.). Academic Press, New York. pp. 97-132.

Parysek, L. M., J. J. Wolosewick, and J. B. Olmsted. 1984. MAP-4: a microtubule-associated protein specific for a subset of tissue microtubules. J. Cell Biol. 99(6): 2287-2296.

Pickett-Heaps, J., T. Spurck, and D. Tippit. 1984. Chromosome motion and the spindle matrix. J. Cell Biol. 99(1): 137-143.

Repetto-Antoine, M., J. De Mey, and V. Meininger. 1982. In situ distribution of microtubules in the rat tectal plate at the earliest stages of cell differentiation using indirect immunofluorescence. Biol. Cell 44: 325- 328.

Reynolds, E. S. 1963. The use of lead citrate at high pH as an electron opaque stain in electron microscopy. J. Cell Biol. 17: 208-212.

Rodning, C. B., S. L. Erlandson, H. D. Coulter, and I. D. Wilson. 1980. Immunohistochmical localization of IgA antigens in sections embedded in epoxy resin. J. Histochem. Cytochem. 28(3): 199-205.

Salazar, H. 1964. Diethylene glycol distearate embedding and ultramicrotome sectioning for light microscopy. Stain Technol. 39: 13-17.

Schliwa, M. 1982. Chromatophores: their use in understanding microtubule-dependent intracellular transport. In Methods in cell biology. Volume 25. The cytoskeleton. Part B. L. Wilson (ed.). Academic Press, New York. pp. 285-312.

Schliwa, M. 1984. Mechanisms of intracellular organelle transport. In Cell and muscle motility. Volume 5. The cytoskeleton. J. W. Shay (ed.). Plenum Press, New York. pp 1-82.

Schliwa, M., and J. van Blerkom. 1981. Structural interaction of cytoskeletal components. J. Cell Biol. 90(1): 222-235.

Schreiner, B. 1977. Vitellogenesis in the milkweed bug, Oncopeltus fasciatus Dallas (Hemiptera). A light and electron microscope investigation. J. Morph. 151: 35-80.

Sharma, K. K., and H. Stebbings. 1985. Electrophoretic characterization of an extensive microtubule-associated transport system linking nutritive cells and oocytes in the telotrophic ovarioles of Notonecta glauca. Cell Tissue Res. 242: 383-389.

Singer, S. J., and A. Kupfer. 1986. The directed migration of eukaryotic cells. Ann. Rev. Cell Biol. 2: 337-365.

Stebbings, H. 1971. Influence of vinblastine sulphate on the development of microtubules and ribosomes in telotrophic ovarioles. J. Cell Sci. 8: 111-125.

Stebbings, H. 1975. The role of microtubules in the assembly of vinblastine-induced crystals. Cell Tissue Res. 159: 141-145.

Stebbings, H., and J. H. M. Willison. 1973. Structure of microtubules: a study of freeze-etched and negatively stained microtubules from the ovaries of Notonecta. Z. Zellforsch. 138: 387-396.

Stebbings, H., and C. E. Bennett. 1976. The effect of colchicine on the sleeve element of microtubules. Exp. Cell Res. 100: 419-423.

Stebbings, H., and C. Hunt. 1982. The nature of the clear zone around microtubules. Cell Tissue Res. 227: 609-617.

Stebbings, H., and C. Hunt. 1983. Microtubule polarity in the nutritive tubes os insect ovarioles. Cell Tissue Res. 233: 133-141.

Stebbings, H., and C. Hunt. 1985. Binding of axonemal dynein to microtubules comprising the cytoplasmic transport system in insect ovarioles. Cell Biol. Int. Rep. 9(3): 245-252.

Stebbings, H., K. K. Sharma, and C. Hunt. 1986. Microtubule-associated proteins in the ovaries of hemipteran insects and their association with the microtubule transport system linking nutritive cells and oocytes. Eur. J. Cell Biol. 42: 135-139.

Taleporos, P. 1974. Diethylene glycol distearate as an embedding medium for high resolution light microscopy. J.Histochem. Cytochem. 22(1): 29-34.

Telfer, W. H. 1975. Development and physiology of the oocyte-nurse cell syncytium. Adv. Insect Physiol. 11: 223-320.

Towbin, H., T. Staehelin, and J. Gordon. 1979. Electrophoretic transfer of proteins from polyacrylamide gels to nitrocellulose sheets: procedure and some applications. Proc. Natl. Acad. Sci. USA. 76(9): 4350-4354.

Tucker, J. B. 1979. Spatial organization of microtubules. In Microtubules. K. Roberts, & J. S. Hyams (eds.). Academic Press, London. pp. 315-357.

Tucker, J. B. 1984. Spatial organization of microtubule-organizing centers and microtubules. J. Cell Biol. 99(1): 55s-62s.

Vallee, R. B., M. J. DiBartolomeis, and W. E. Theurkauf. 1981. A protein kinase bound to the projection portion of MAP-2 (microtubule-associated protein 2). J. Cell Biol. 90(3): 568-576.

Valnes, K., and P. Brandtzaeg. 1981. Unlabeled antibody peroxidase-antiperoxidase method combined with direct immunofluorescence. J. Histochem. Cytochem. 29(6): 703-711.

Valnes, K., and P. Brandtzaeg. 1985. Retardation of immunofluorescence fading during microscopy. J. Histochem. Cytochem. 33(8): 755-761.

Vanderberg, J. P. 1963. Synthesis and transfer of DNA, RNA, and protein during vitellogenesis in Rhodnius prolixus (Hemiptera). Biol. Bull. 25: 556-575.

Watson, A. J. 1984. The dynamics of the Rhodnius prolixus follicle cell cytoskeleton: ultrastructure and immunocytochemistry. M. Sc. thesis. Department of Zoology, University of Manitoba, Canada. 146 p.

Watson, A. J., and E. Huebner. 1986. Modulation of cytoskeletal organization during insect follicle cell morphogenesis. Tissue Cell 18(5): 741-752.

Webb, B. C., and L. Wilson. 1980. Cold-stable microtubules from brain. Biochem. 19(9): 1993-2001.

Weber, K., P. C. Rathke, and M. Osborn. 1978. Cytoplasmic microtubular images in glutaraldehyde-fixed tissue culture cells by electron microscopy and by immunofluorescence microscopy. Proc.Natl. Acad. Sci. USA 75(4): 1820-1824.

Weber, K., and M. Osborn. 1979. Intracellular display of microtubular structures revealed by indirect immunofluorescence microscopy. In Microtubules. K. Roberts, & J. S. Hyams (eds.). Academic Press, London. pp. 279-313.

Weisenberg, R. C. 1972. Microtubule formation in vitro in solutions containing low calcium concentrations. Science 177: 1104-1105.

Winter, H. 1974. Ribonucleoprotein-Partikel aus dem telotroph-meroistischen var von Dysdercus intermedius Dist. (Heteroptera, Pyrrhoc.) und ihr Verhalten im zellfreien Proteinsynthesesystem. Wilhelm Roux's Arch. 175: 103-127.

Winter, H., D. Wiemann-Weiss, and F. Duspiva. 1977. Endogene Synthese kurzlebiger Messenger-RNS in der Oocyte von Dysdercus intermedius Dist. nach Abschluss der Vitellogenese. Wilhelm Roux's Archiv. 182: 39-58.

Wolosewick, J. J. 1980. The application of polyethylene glycol (PEG) to electron microscopy. J. Cell Biol. 86(2): 675-681.

Wolosewick, J., and J. De Mey. 1982. Localization of tubulin and actin in polyethylene glycol embedded rat seminiferous epithelium. Biol. Cell 44: 85-88.

Zinsmeister,P. P., and R. Davenport. 1971. An autoradiogaphic and cytochemical study of cellular interactions during oogenesis in the milkweed bug, Oncopeltus fasciatus. Exp. Cell Res. 67: 273-278.